Resilience Development Initiative

Paper Competition Compilation Book:

Bridging Earth Science and Sustainability: The Net Zero Emission Geoscience Challenge

RDI Special-Ed Working Paper No. 4 (REER) 20250611

Paper Competition Compilation Book:
Bridging Earth Science and Sustainability: The Net Zero Emission Geoscience Challenge

Compiled by:
IUGC ITB 2024 Team and Resilience Development Initiative (RDI)

Authors (alphabetical order):

Aleena Fauzia Warda
Ardelia Khadar Kinasih
Azzahra Amalliya
Davina Mutiara
Ekasari Nurkholijah
Ellysa Dinda Nathasya
Hassanna Dita Padang
Kania Humaira Ibrahim
Safira Alya Harsyarani
Savira Zahrul Khumairo
Sultan Daffa Khoirussyah Suhardi
Yuniar Ramadhani

Editors:
Chelsea Patricia
Evita Mahar Dewi
Baihaqi Muhammad
Rr. Widiartyasari Prihatdini

Design and Layout:
Salma Lathifah

Publisher:
Resilience Development Initiative (RDI)

Competition Organiser:
IUGC ITB 2024

This publication is a compilation of the winning papers from the Paper and Poster Competition held as part of the International Undergraduate Geophysics Competition (IUGC) ITB 2024 on September 15, 2024. It highlights the diverse and innovative ideas contributed by undergraduate students in the field of geoscience across Indonesia, with a shared vision of achieving net-zero emissions and promoting sustainability.

We would like to extend our sincere gratitude to all participants and winners who have contributed their time, creativity, and dedication to this competition. Your work exemplifies the spirit of collaboration and innovation that is essential in addressing global sustainability challenges.

Publication Date:
June 2025

Table of Contents

Part I: Geothermal Innovations

Modified-Binary System: Improving Binary System Power Plant Using Bacillus subtilis Bacteria and Zeolite Li-X for Improving LUSI Geothermal Potential

Ardelia Khadar Kinasih[1], Sultan Daffa Khoirussyah Suhardi[1], Yuniar Ramadhani[1]

[1] *Geophysical Engineering, Institut Teknologi Sepuluh Nopember*

Abstract

The hot mud eruption in Sidoarjo (*Lumpur Sidoarjo*/LUSI) since 2006 has become a significant environmental and social issue. The eruption, affecting approximately 30,000 residents, has led to extensive infrastructure disruptions and severely impacted air quality. The continuously increasing volume of hot mud, along with the gases emitted, including methane (CH_4) and carbon dioxide (CO_2), contributes to environmental degradation and poses ongoing challenges and health risks to the local population. Nevertheless, the hot, mineral-rich fluid from the eruption could be harnessed as a low-temperature geothermal resource. Recent studies have revealed that the LUSI mudflow contains substantial lithium content, which is a potential material to explore as a sustainable energy source, utilising advanced techniques. The optimisation of the hot fluid using specialised bacteria such as *Bacillus subtilis* is studied in this paper, which can effectively reduce its viscosity and make it easier to process. Additionally, the separation of CH_4 and CO_2 can be achieved using a Zeolite Li-X separator, although in return it also reduces CO_2 levels by nearly 77% and CH_4 by almost 15.1%. Consequently, this process enables CH_4 to be utilised as a renewable biogas option. The implementation of a Modified-Binary System processing system, incorporating a separator before the heat exchanger, offers a promising approach to convert the mudflow disaster into a potentially sustainable energy innovation. This approach addresses environmental concerns and provides a viable solution for utilising geothermal resources effectively.

Keywords: *Bacillus, Binary, Geothermal, Lumpur Sidoarjo*

Introduction

On May 29, 2006, a sudden eruption of mud and gases emerged from a vent near a hydrocarbon exploration well in Sidoarjo, East Java, Indonesia (**Figure 1**). This event, termed the LUSI (*Lumpur Sidoarjo*) mud volcano, has been persistently active, discharging mud up to 160,000 m^3 daily. Prior to the incident, an eruption occurred near the Banjar Panji-1 (BJP-1) well, which was drilled to a depth of 2.8 km by PT Lapindo. Following the initial eruption, another subsequent minor eruption along a 1 km stretch of a northeast-trending fracture zone occurred. The primary eruption site, approximately 200 meters southwest of the BJP-1 well, remains active and emits mudflow until now. The well had penetrated over-pressured and under-compacted Pleistocene sediments below 1.3 km. It is predicted that the absence of casing below 1 km contributed to the fracturing. The eruption may also have been influenced by a magnitude 6.2 earthquake that occurred in Central Java two days prior, approximately 200 km away (Hochstein and Sudarman, 2010)

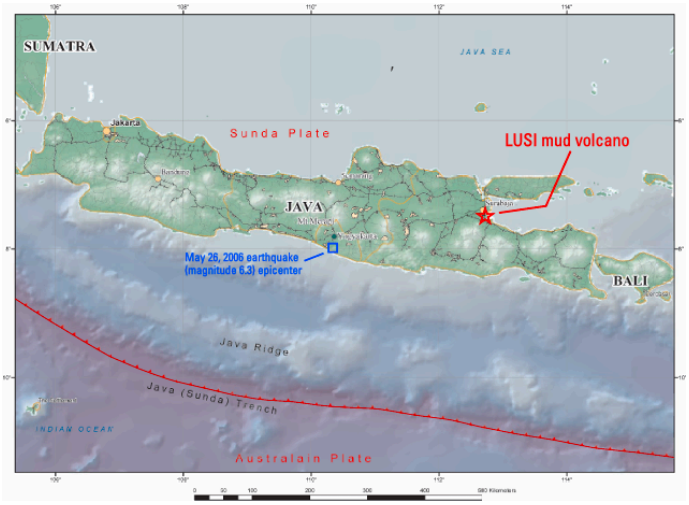

Figure 1. A map of Java illustrates the position (indicated by a star) of the LUSI mud volcano in eastern Java, south of Surabaya. The blue square marks the epicentre of the Yogyakarta earthquake that occurred on May 26, 2006. The map is based on data from the U.S. Geological Survey (2006) (Plumlee et al., 2008).

The LUSI mud eruption has significantly disrupted the surrounding environment and society. Approximately 30,000 residents have been affected, with extensive damage to infrastructure and displacement of communities. The eruption has also severely impacted air quality due to the emission of greenhouse gases, including methane (CH_4) and carbon dioxide (CO_2), which exacerbate local pollution and pose health risks. The continuous flow of hot mud and the release of these gases have complicated environmental management and highlighted the urgent need for innovative solutions. Aside from addressing these critical environmental challenges, research focusing on LUSI's material also presents an opportunity for sustainable energy development due to its unique condition.

The LUSI mud is approximately 60% water and 40% siliciclastic (Mazzini et al., 2007). It has a temperature of up to 100 °C, is dominantly composed of clay, and has a lesser percentage of smectite, illite, and chlorite. Feldspars, quartz, and organic materials were also found in the LUSI mud, with calcium carbonate and iron sulfide in trace amounts, which

make up the overall composition. Previous studies found that abiotic CO_2 and biotic CH_4 content dominate the LUSI composition, which is thought to occur due to active tectonic activity meeting heat flows. The chemical composition of the LUSI also consisted of dissolved Cl^-, Na^+, and some amount of Li and B compounds in its water content, which is thus called hydrothermal water (Mazzini et al., 2018). LUSI resembles a modern eruptive sediment-hosted geothermal system (SHGS), which has similarities to 'classic' mud volcanoes that occur due to high pressure from the flow of hydrothermal fluid from heated sedimentary rock (especially mudstone) through the rock pores (Mazzini and Etiope, 2017). The analysed hydrothermal fluid flow begins to form and rises upward at a depth of 1.3 km, allowing the presence of sediment at high temperatures.

Given the substantial lithium content in the LUSI and thus present geothermal potential, the site offers a promising avenue for alternative energy. The hot, mineral-rich fluids from the eruption could serve as a low-temperature geothermal resource. Optimisation of LUSI's geothermal potential is possible by applying advanced technologies, such as *Bacillus subtilis* bacteria, which can break down hydrocarbon compounds, reduce mud viscosity, and using Zeolite Li-X separators to separate CH4 and CO2 efficiently. These technologies, integrated into a Modified-Binary System, could enhance geothermal energy extraction efficiency while addressing environmental concerns. This innovative approach not only aims to mitigate the adverse effects of the eruption but also seeks to harness the geothermal potential of LUSI, turning a disaster into a sustainable energy solution. This research will explore these methodologies and their integration into the Modified-Binary System. Through developing effective methods for utilising the geothermal potential of LUSI, it is also possible to address the environmental and energy challenges in the region.

Theoretical Framework

2.1 Geothermal Reservoir Type

The geothermal wells in the LUSI field produce high-temperature dry steam, which is highly advantageous for electricity generation. There are several types of geothermal fluid found at depths of approximately 1 km, with their respective technology for power generation:

High-temperature geothermal reservoirs contain fluids with temperatures exceeding 225°C (Saptadji, 2018). They are typically associated with features such as fumaroles, steam vents, mud pools, and highly altered ground. Geothermal fluids at these high temperatures are commonly utilised for electricity generation.

Medium-temperature geothermal reservoirs have hot fluid temperatures ranging from 125°C to 225°C. Geothermal fluids within this temperature range are effectively used for electricity generation through the Flash Steam Power Plant system, which performs efficiently under such conditions.

Low-temperature geothermal reservoirs are characterised by fluid temperatures below 125°C and are often associated with hot or warm springs. The most common technology for

harnessing low-temperature geothermal energy is binary cycle power generation (Saptadji, 2018), which may involve steam turbine condensation as part of the process.

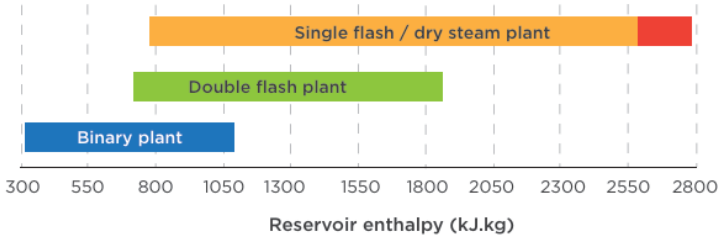

Figure 2. Plant Type and Reservoir Enthalpy (Zarrouk & Moon, 2014)

2.2 LUSI Geological and Stratigraphic

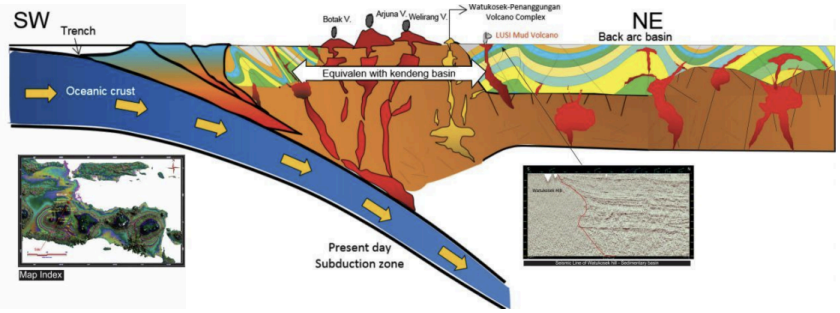

Figure 3. Geological cross-section model of LUSI that has correlation with the Watukosek-Penanggungan volcanic complex (Wibowo et al., 2018).

The LUSI is situated in the Kendeng Basin, approximately 10 km N-E from the Watukosek-Penanggungan volcanic complex (Clements et al., 2009). Based on its geological conditions, the LUSI incident is located in a back-arc basin zone of the complex, mainly affected by the Watukosek Fault, which imposes a principal stress direction of Northeast to Southwest and Northwest to Southeast. This stress regime is evident from the deformation and alignment patterns observed in the region, including the change in direction of the Porong River at the incident site. Specifically, the river's deviation aligns with the orientation of the Watukosek Fault, indicating a strong structural control by fault activity and the associated stress field in this area (Wibowo et al., 2018). The emergence of mud over the surface is thought to be caused by the high rate of sedimentation around LUSI, about 2,480 m/s, which contributes to an overpressure in the Kendeng zone (Kadar et al., 2007). An overpressure is caused by a high sedimentation rate, where the Kendeng zone is dominated by alluvial deposits that are not fully compacted (Willusmen et al., 1994). All geopressured sediments become saturated and compressed, forming a mud diapir that then penetrates the overlying sediment layers (Wibowo et al., 2018), thus creating a mudflow.

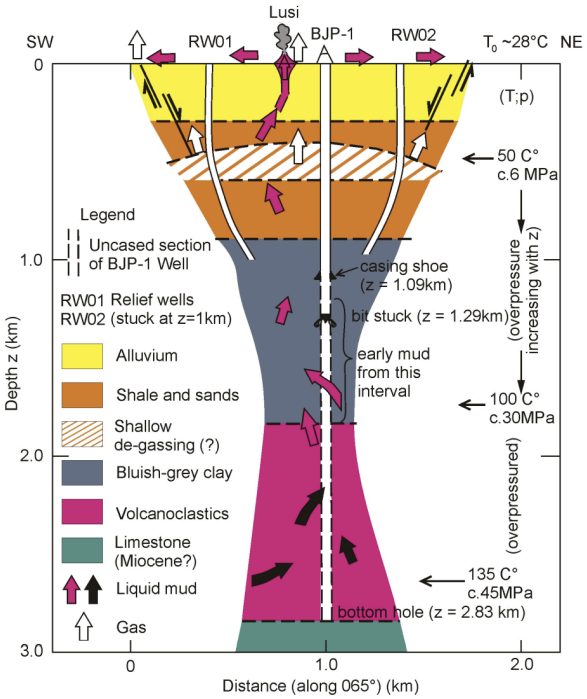

Figure 4. Geological model based on the BJP-1, RW01, and RW02 models shows the possible lithology from the reservoir data (Hochstein and Sudarman, 2010).

Previous studies on the BJP-1 well (Mazzini et al., 2007; Davies et al., 2008) have mentioned different temperatures and porosity at varying depths in the well. The temperature at a depth of 2,667 m is 138°C, while at 1,700 m it is 100°C, as recorded in Figure 4. An unconsolidated reservoir with easily crumbled bluish-grey clay deposits with plastic found at depths of 1,200 to 1,850 m. This formation undergoes pressure of 20-30 MPa with porosity over 35%. The porosity is 20% under the condition of 45 MPa, 135°C, below 1,850 m. This data obtained a geothermal gradient value of 42°C/km (Mazzini et al., 2007). Thus, the mud contained within the reservoir is estimated to have a density of less than 1,730 kg/m³, with the particle density expected to be between 2,500 and 2,600 kg/m³, indicating a liquid content of over 50% (Hochstein & Sudarman, 2010).

The geological conditions of LUSI's potential as a geothermal spot, characterised by an overpressured reservoir and geology dominated by sediments, indicate a geopressured reservoir. The presence of the Watukosek Fault structure, oriented NE-SW and NW-SE, indicates the location as a weak zone. This type of geological system suggests that LUSI's geothermal system is classified as unconventional.

2.3 Geochemistry Analysis

The determination of a geothermal system also requires substantial information through the chemical composition of the mud, specifically by analysing the presence of Hydrogen-2 (^{2}H or deuterium (D)), Oxygen-18 (^{18}O), and Carbon-13 (^{13}C). Analysing isotopes aims to determine the geothermal fluid's origin and type and estimate the subsurface temperature (Sutaningsih, 2010). To determine these values, a geothermometer calculation is performed using the following formula (Blattner and Hoefs, 1994):

$$\Delta^{13}CCO_2 - CH_4 = \frac{15650}{(t°C)+168)} - 9$$

$$t(°C) = \frac{15650}{(t°C)+\Delta^{13}CCO_2-CH_4)} - 168 \quad (1)$$

As previously discussed, LUSI's chemical content is mostly SiO_2 which comes from clay, feldspar minerals, and quartz. The dominance of clay in LUSI increases Al_2O_3, Fe_2O_3, and K_2O content. Na_2O and MgO were also found quite abundantly due to the copresence of feldspar and dolomite respectively, where CaO carried by calcite minerals in quite considerable amounts (Ali A. J., 2007).

2.4 Binary System Power Plant

In general, geothermal fluids need to have a temperature above 200°C to be utilised for electricity generation, whereas geothermal fields with temperatures of 20 to 100°C are more suitable for direct use. However, the binary system power plant technology allows the utilisation of medium to low temperature reservoirs.

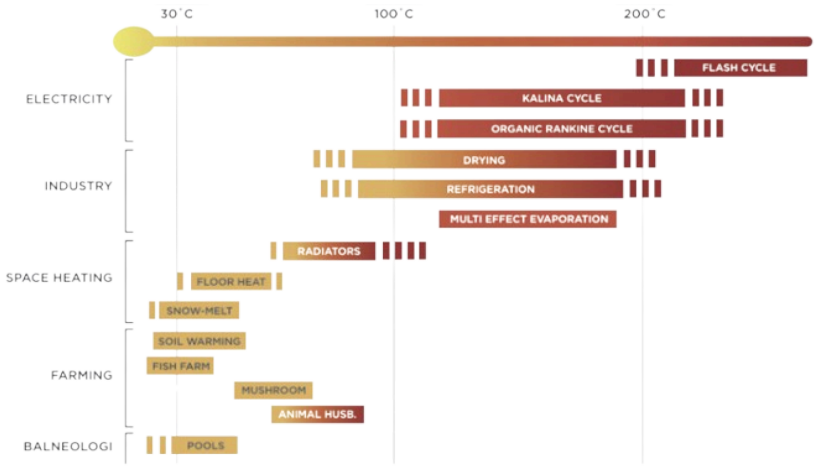

Figure 5. Temperature diagram showing the common usage of each temperature range

The binary system power plant (**Figure 6**) utilises two types of working fluids: geothermal fluid and organic fluid. The organic fluid will evaporate due to its heat transfer from the geothermal fluid within the heat exchanger system. The vapour produced by the organic fluid will drive the turbine, generating electricity in the generator. This process is also known as the Organic Rankine Cycle (ORC).

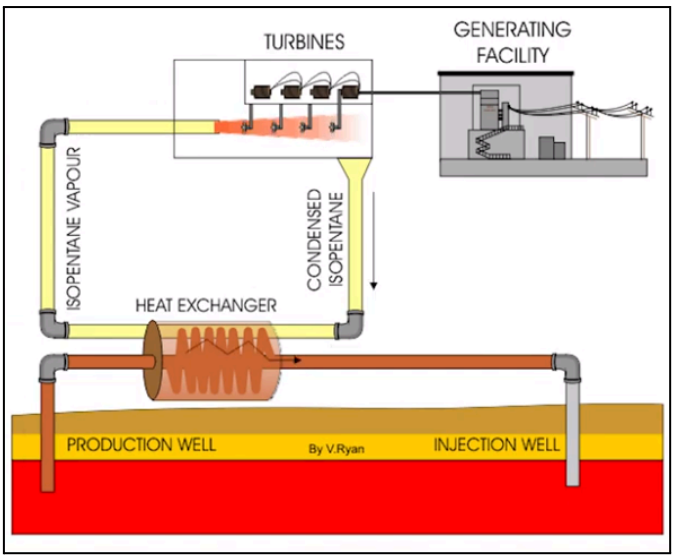

Figure 6. Common binary cycle power plant

To drive the turbine, an appropriate quality of organic fluid must be used so that it can vaporise at the temperature produced by the geothermal fluid. The selection of the organic fluid is not arbitrary. There are several criteria for organic fluids based on toxicity, flammability, Ozone Depletion Potential (ODP), and their effects on global warming (GWP).

Table 1. Organic fluid that is used for the binary cycle

Fluid	Formula	Toxicity	Flammability	ODP	GWP	T°C	Thermal Efficiency			Utilization Efficiency		
							93°C	149°C	204°C	93°C	149°C	204°C
R-12	$CC_{12}F_2$	non-toxic	non-flam	1.0	4.500	-	-	-	-	-	-	-
R-14	$C_2C_{12}F_4$	non-toxic	non-flam	0.7	5.850	-	-	-	-	-	-	-
Propane	C_3H_8	low	very high	0	3	96.95	-	-	-	-	-	-
i-Butane	i-C_4H_{10}	low	very high	0	3	135.92	5.5	10.3	-	1.9	48.8	-
n-Butane	C_4H_{10}	low	very high	0	3	150.8	-	-	-	-	-	-
i-Pentane	i-C_5H_{12}	low	very high	0	3	187.8	5.2	9.8	13.7	30.5	44.6	57.7
n-Pentane	C_5H_{12}	low	very high	0	3	193.9	-	-	-	-	-	-
Ammonia	NH_3	toxic	lower	0	0	133.65	-	-	-	-	-	-
Water	H_2O	non-toxic	non-flam	0	-	374.14	-	-	-	-	-	-

Source: DiPippo, R. (2012).

The ODP and GWP levels of the organic fluids or working fluids R-12 and R-114 are the highest, which led to their ban by the Copenhagen Amendment (1994). Global Warming Potential (GWP) is a measure of how much heat a greenhouse gas traps in the atmosphere over a specific time period (usually 100 years) compared to carbon dioxide (CO_2), which is

assigned a baseline value of 1.0. A GWP of 1.0 for CO_2 means it is used as the reference gas to evaluate the warming impact of other gases. While CO_2 itself can be used as a working fluid due to its low toxicity and non-flammability, its GWP of 1.0 still contributes to greenhouse gas emissions and thus limits its applicability in sustainable systems (DiPippo, 2012).

2.5 Zeolite Li-X Adsorbent as CO_2 and CH_4 Separator

Zeolite has become one of the promising materials for separating CO_2 from CH_4 due to its unique porous structure and selective adsorption properties. One of the key parameters that determines the adsorption behavior of zeolite is the silicon-to-aluminum (Si/Al) ratio, which reflects the framework composition and charge distribution within the crystal lattice. A lower Si/Al means higher Al content. Zeolites characterised by low Si/Al ratio exerts superior CO_2 binding in pressure as low as 1 bar (14.5 psi), with having poorer CO_2 adsorption capacity in higher pressure conditions (e.g., 5 bar ~ 72.5 psi) (Bonenfant et al., 2008) The use of zeolite with a lower Si/Al ratio allows its structure to become hydrophobic due to the minimal silicon content in the zeolite's crystal structure (Boer et al., 2023).

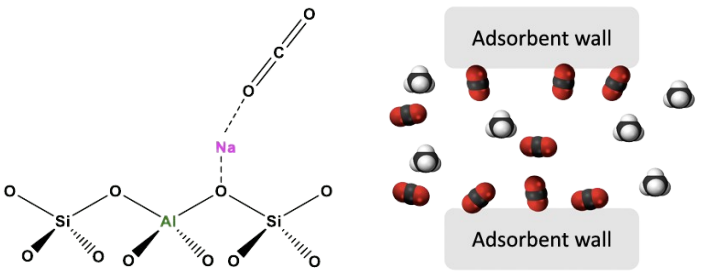

Figure 7. (A) The ability of zeolite to bind CO_2 based on its chemical structure; (B) Zeolite adsorption to CO_2 (red) and CH_4 (white) diffusing (Boer et al., 2023).

Additionally, the ability of zeolite to trap CO_2 also depends on its pore size. Zeolite of type X has large to medium pores, which results in an equilibrium separation adsorption. Zeolite Li-X is used to separate methane (CH_4) and carbon dioxide (CO_2) based on its superior adsorption properties and structural characteristics. Zeolite Li-X, a synthetic aluminosilicate with a well-defined crystalline structure, is particularly effective due to its ion-exchange capacity and specific pore geometry. This material features a network of interconnected aluminosilicate tetrahedra, creating pores that facilitate selective adsorption. The lithium ions in Zeolite Li-X enhance the adsorption of CO_2 through electrostatic interactions and van der Waals forces, thereby allowing CH_4 to be more efficiently separated. In the separation process, a gas mixture is passed through a column packed with Zeolite Li-X, where the zeolite selectively adsorbs CO2. This selective adsorption allows for the efficient recovery of methane, which can be utilised for biogas production, while simultaneously managing CO_2 emissions (Boer et al., 2023).

The adsorption capacity of CH_4 and CO_2 from zeolite can also be calculated using the equation employed in the calculation of sulfur adsorption (Long et al., 2015) with the following formula:

$$C_a = \frac{v \times \int_{t0}^{t1} (C_{in} - C_{out}) \times M \times 10^{-3}}{V_{mol} \times m_s} \quad (2)$$

Where C_a represents the adsorption capacity of the zeolite, v is the inlet gas flow rate (L/min), t is the heating time of the zeolite, C_{in} and C_{out} are the inlet and outlet concentrations of the fluid passing through the zeolite (ppmv), M is the molar mass of the fluid passing through the zeolite (g/mol), ms is the weight of the adsorbent (g), V_{mol} is the molar volume (L/mol at 25°C, 1 atm), and 10^{-3} is the normalisation coefficient used to convert various units to be consistent. This formula will be used to calculate the adsorption rate of the zeolite being utilised.

To maximise the use of zeolite, the addition of potassium hydroxide (KOH) is necessary to increase the amount of CH_4 that passes through the separator system. The use of KOH up to 30% can increase the CH_4 content by 60.5% (Kusumawati and Nur, 2015) due to the hydrogenotrophic methanogenesis reaction caused by the breakdown of H_2 and C from H_2S and CO_2 when trapped in the zeolite under base conditions (Peters et al., 1995). The zeolite also needs to be heated for several minutes to hours to achieve optimal results in the adsorption process.

2.6 Application of *Bacillus subtilis* Bacteria

Bacillus subtilis is a highly adaptable bacteria that can be found in various habitats, including both terrestrial and aquatic environments. *Bacillus subtilis* also can thrive in diverse conditions by forming a resistant dormant endospore to nutrient deficiencies and other environmental stresses (Earl et al., 2008). *Bacillus subtilis* can produce biosurfactant, an amphipathic molecule with both polar (hydrophilic) and nonpolar (lipophilic) regions, which plays a crucial role in enhancing the wettability of fluids (Dhail, 2013).

Ni'matuzahroh et al. (2019) found that biosurfactants produced by *Bacillus subtilis*, called surfactin, are highly effective in reducing the viscosity of oil sludge. The testing of surfactin is appropriately done at over 70°C, which Takahashi et al. (2011) stated that temperature significantly influences the viscosity of mud, which is known to reduce surface tension by up to 40 mN/m. Biosurfactant production can be maximised by maintaining the stability of temperature, pressure, and pH in the surrounding environment (Pacwa-Plociniczak et al., 2011). The formation of surfactin is also influenced by salt concentration and limited oxygen levels. Surfactin from *Bacillus subtilis* bacteria can be injected directly into isolation tubes without the need for special treatment, thereby reducing production costs.

Method

3.1 Modified-Binary System

Utilising resources from the LUSI field will adopt the modification of the Binary Power Plant system, which is expected to yield energy resources beyond heat. As a geopressure field originating from sedimentary deposits, LUSI contains CH_4, which is rarely found in other conventional geothermal fields. The design of this Modified Binary System can be seen in **Figure 8**, which shows the process of isolating and separating Non-Condensable Gas (NCG) through an adsorbent, zeolite separator. *Bacillus Subtilis* will be placed in the isolation chamber to reduce the viscosity of the hot mud.

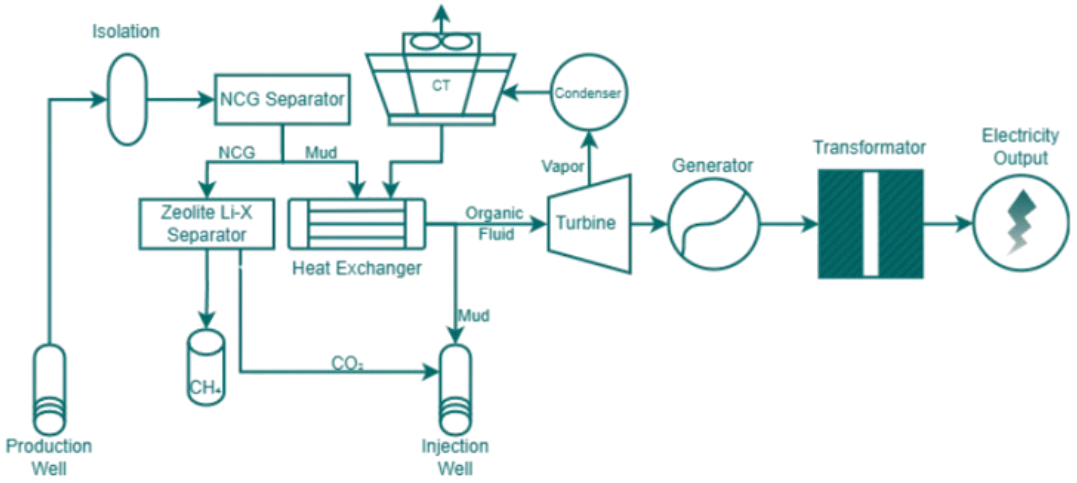

Figure 8. Modified-Binary System Scheme Sketch

To achieve more optimal results, a 70 kilogram zeolite was heated for 5,760 minutes (about 4 days) (Manullang et al., 2019). The zeolite's adsorption capacity was adjusted according to the results from Boer et al. (2023), with values of 7.0 mmol/g for CO_2 and 0.5 mmol/g for CH_4.

To determine how much electrical energy can be produced from the LUSI reservoir, the following calculation is used (Tanbar et al., 2022):

$$H_{ei} = A.h[(1 - \phi)\rho_r c_r T_i + \phi(S_L \rho_L u_L + S_v \rho_v u_v)_i] \quad (3)$$

$$H_{ef} = A.h[(1 - \phi)\rho_f c_f T_f + \phi(S_L \rho_L u_L + S_v \rho_v u_v)_f] \quad (4)$$

$$H_{th} = H_{ei} - H_{ef} \quad (5)$$

$$H_{de} = R_f H_{th} \quad (6)$$

$$H_{thermal} = \frac{H_{de}}{t \times 365 \times 24 \times 3600} \quad (7)$$

$$H_{el} = \eta \times H_{thermal} \quad (8)$$

Equations (3) and **(4)** are used to measure the initial and final energy values of a geothermal resource, respectively. **Equation (5)** determines the maximum energy that can be utilised from the geothermal field. **Equations (6)** and **(7)** are used to assess the practical geothermal energy that can be utilised and the duration of its usability. Finally, **Equation (8)** is used to calculate the electric potential.

This equation requires data including the reservoir area A (in m^2), initial and final reservoir temperatures T_i and T_f (in ^oC), rock porosity $\boldsymbol{\phi}$ (fraction), rock heat capacity C_r (kJ/kg^{o}C), and densities for rock ϱ_r, water ϱ_L, and steam ϱ_V (in kg/m^3). Additionally, saturation values for both fluid and steam are needed for the calculations. If the reservoir does not produce steam, the calculation for steam is excluded. Furthermore, a recovery factor R_f of 0.5 and an electrical conversion factor of 0.14 are used for medium-temperature reservoirs (Tanbar et al., 2022).

The efficiency of the binary system will also be calculated using the Carnot formula, as follows (DiPippo, 2012):

$$\eta_{cc} = \eta_{max} = 1 - \frac{T_L}{T_H} \quad (9)$$

This will allow us to determine the maximum efficiency at a sink temperature (T_L) of 40 ^{o}C.

3.2 Flowchart

Here are the steps for processing LUSI mud using the Modified-Binary System.

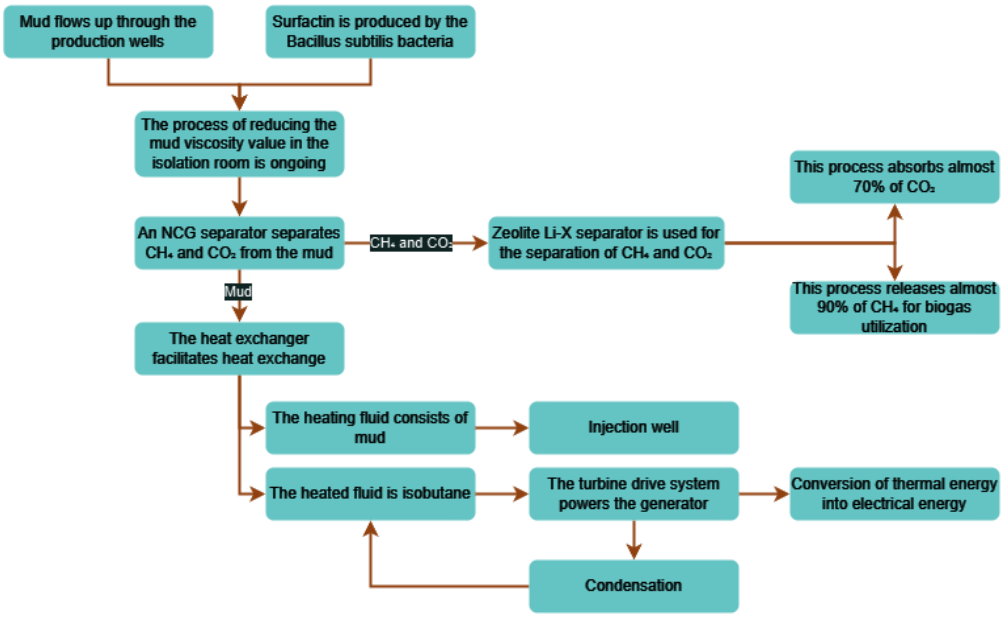

Figure 9. Modified-Binary System Workflow

Data and Results

The data obtained from research conducted by Sutaningsih et al. (2010) shows the presence of ^{13}C, ^{2}H, and ^{18}O used to determine the characteristics of the fluids within the LUSI reservoir. **Table 2** shows the percentage and molarity ^{13}C in various hydrocarbon gases (e.g., C_1, C_2, C_3, CO_2, etc.) sampled from different locations around the LUSI mud volcano. Data from **Table 3** indicates the presence of chemical content in the form of deuterium (^{2}H), with a range from -17.5% to -2.7% and a deviation in the concentration of ^{18}O from +5.28% to +10.11% at the eruption site, which is suspected to be associated with igneous rocks originating from magma. Another sample was taken from a well location, with ^{2}H concentrations ranging from -61.5% to -3.4% and ^{18}O ranging from -9.85% to +1.64%. This data indicates meteoric water contaminated by fluids originating from the eruption centre.

Table 2. ^{13}C percentage and molarity of LUSI mud composition

Composition	Jatirejo		Wunut		Jabon		SCJ		SSJ		Ketapang		SSK		Mindi		MBG		SBT	
	d-13C (%)	Mol (%)	d-13C (%)	Mol (%)	d-13C (%)	Mol (%)	d-13C (%)	Mol (%)	d-13C (%)	Mol (%)	d-13C (%)	Mol (%)	d-13C (%)	Mol (%)	d-13C (%)	Mol (%)	d-13C (%)	Mol (%)	d-13C (%)	Mol (%)
C1	-37.30	57.18	-37.14	67.64	-37.60	39.93	-39.65	50.94	-36.67	54.99	-36.89	83.98	-41.26	53.51	-41.48	53.72	-41.46	42.39	-41.25	54.10
C2	-26.02	2.41	-26.10	2.93	-26.26	1.81	-26.11	0.78	-26.13	2.60	-25.84	0.86	-30.32	2.45	-30.56	2.64	-30.60	2.10	-30.58	2.64
C3	-24.36	0.95	-24.72	1.20	-24.53	0.76	-23.99	1.24	-23.95	1.08	-23.88	1.17	-27.66	1.05	-27.80	1.12	-27.90	0.90	-27.15	1.14
iC4	-25.43	0.19	-25.34	0.25	-25.51	0.15	-25.03	0.22	-24.86	0.19	-24.78	0.22	-28.49	0.18	-28.84	0.21	-29.21	0.17	-27.45	0.22
C4	-23.20	0.10	-22.72	0.15	-22.94	0.11	-23.89	0.20	-22.84	0.20	-22.27	0.11	-26.61	0.20	-26.84	0.20	-27.26	0.16	25.80	0.21
iC5	-	0.03	-	0.05	-	0.03	-	0.06	-	0.05	-	0.02	-	-	-	-	-	-	-	-
C5	-	0.00	-	0.00	-	0.00	-	0.03	-	0.03	-	0.01	-	-	-	-	-	-	-	-
C6+	-	0.04	-	0.53	-	0.28	-	0.02	-	0.03	-	0.02	-	-	-	-	-	-	-	-
CO_2	-1.08	17.00	-3.60	7.13	-0.07	18.67	-2.93	31.96	-6.03	31.18	-16.14	0.97	-	-	-	-	-	-	-	-
N_2	-	14.63	-	14.27	-	28.81	-	11.58	-	8.62	-	9.46	-	-	-	-	-	-	-	-
O_2	-	7.30	-	6.29	-	9.67	-	2.97	-	1.03	-	3.18	-5.15	34.31	-13.92	34.92	-4.77	34.87	-7.56	48.62

Source: Sutaningsih et al., (2010).

Table 3. Deuterium and ^{18}O composition in LUSI mud volcano

Sample	H-2(Deuterium)	O-18
L-AM-B-1st-3	-15.2±0.7	-0,71±0.45
L-AL-43-1st	-6.6±0.6	8,96±0.35
L-AB-1st	-30,9±0.5	-3.86±0.36
L-AL-45	-11,3±0.5	7,79±0.38
1st-HS-WP-1	-61,5±0.4	-9,85±0.38
L-AM-R-I-2	-41,5±0.6	-4,80±0.43
L-LM-B-IST-I	-35,5±0.7	-2,96±1.19
L-AL-45-ST	-10,8±0.1	8,14±0.35
L-AM-B-1ST	-18,0±0.9	-0.68±0.40
L-AM-RI-1ST-I	-40,0±0.7	-7,46±0.45
L-CJR-1	-35,3±0.7	-7,68±0.37
SPILL WAY	-8,3±0.7	-0,25±1.26
L-AS2-1ST-2	-21,7±0.6	-1,01±1.19
L-AS1-1ST-1	-25,3±0.7	-4,35±0.37
L-ARK-1ST	-3,4±0.7	1,64±1.26
L-LKA-1-1ST	-6,6±0.7	2,61±1.19
L-L-43	-15,4±0.7	7,43±0.37
L-CS-1	-17,5±0.7	5,28±1.26
Bubble Jatirejo	-10,3±0,3	+2,83±0,1
Before outlet Porong (upside)	-37,2±0,6	-5,67±0,3
After outlet Porong (downside)	-37,9±0,7	-6,4±0,3
LP 45 A	-2,7±0,3	+10,11±0,4
LP 45 B	-10,7±0,7	+8,56±0,4
Flamboyan Siring Barat	-47,1±0,8	-7,83±0,4
LP 44	-13,8±0,8	+7,59±0,4

Source: Sutaningsih et al., (2010).

Table 4. Temperature estimated from the ^{18}O, Deuterium, and ^{13}C using geothermometer calculation

Location	T (ºC)	Location	T (ºC)
Jatirejo	514	SCJ-2	510
Wunut	536	SSK	515
Jabon	505	MND	596
SSJ	569	MBG	510
Ketapang	694	SBT-1	535
Mean			548.4

Table 4 shows that the average subsurface temperature of LUSI can be determined through geothermal calculations, which estimate it to be approximately 548.4°C.

Reservoir data was also obtained to determine how much energy can be harnessed from LUSI as a geothermal reservoir. **Equations (3) to (9)** were used to calculate the energy output before and after the reservoir's utilisation. The calculations estimated a reservoir potential of 88.74 MWe, disregarding steam output, as it was assumed that the reservoir produces no steam and consists almost entirely of liquid mud. The efficiency obtained using **Equation (9)** resulted in a maximum efficiency of 29.6% or approximately 30%, which is more efficient compared to conventional reservoirs using the same binary system. Under the same concept, a reservoir with a temperature of 150°C would yield a maximum efficiency of 26% (DiPippo, 2012). Economically, the reservoir could generate an annual revenue of USD 65,209,511.34 with a selling price of 0.097 USD/kWh.

Table 5. Data calculation for LUSI reservoir using volumetric method.

Parameter	Initial	Final	Unit
Area	7		km^2
Thickness	1850		m
Rock Porosity	0.35		Fraction
Rock Density	1730		kg/m^3
Reservoir Temperature	135	100	°C
Water Saturation	0.6	0.46	Fraction
Recovery Factor	0.5		Fraction
Electrical Conversion Factor	0.14		Fraction
Plant Factor	0.9		Fraction
Water Density	840.23	887.01	kJ/kg
Lifetime	30		Year
Electricity Potential	88.73		MWe

Source: Tanbar et al., (2022).

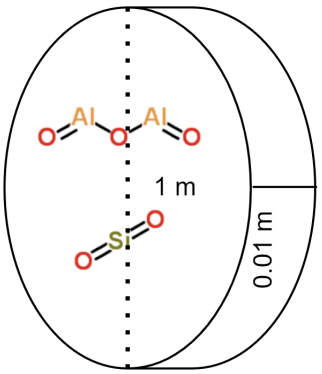

Figure 10. The zeolite membrane idea has a dimension of 0.035 m^3 and is adjusted to the general size of the separator

In this system, LUSI mud flows up through the production wells and passes through the pipe to the isolation room. In the isolation room, there will be a dedicated area for the cultivation of *Bacillus subtilis* bacteria. This area will be kept in closed conditions to prevent oxygen from entering and to maintain stable temperature and pressure. The temperature will be maintained between 35°C-37°C to optimise surfactin production from the bacteria. The surfactin produced by the *Bacillus subtilis* bacteria will then be added to and mixed with the mud in the isolation room. This process aims to reduce the viscosity of the LUSI mud, making it easier to proceed to the next stage. The process then continues with the Non-Condensable Gas (NCG) separator.

The Non-Condensable Gas (NCG) separator uses a two-phase separator to separate the hot fluid (liquid phase, LUSI mud) from the vapour phase (CH_4 and CO_2). The separation process occurs when the LUSI mud, which already has a low viscosity, enters the NCG separator at a temperature of approximately 180°C. The mud then experiences very high centrifugal force, causing CH_4 and CO_2 to rise to the separator walls and continue to the Zeolite Li-X separator. Meanwhile, the remaining mud, which settles at the bottom of the separator, flows directly to the heat exchanger. The compounds are further separated when CH_4 and CO_2 enter the Zeolite Li-X separator. The Zeolite Li-X separator is designed to operate at low pressure, as this ensures the highest quality zeolite content. Additionally, the low Si/Al ratio in the zeolite requires appropriate pressure conditions, specifically 1 bar or 14.5 psi, to maintain its effectiveness. The zeolite will bond with CO_2, and in subsequent stages, the CO_2 can be separated from the zeolite and reinjected into the reservoir via an injection well to maximise future production. Meanwhile, CH_4 will flow into a storage tube, where it can be used for biogas production.

After passing through the separation process in the NCG separator, LUSI mud will enter the heat exchanger. A working fluid, such as butane, is used in this process. Since the temperature of the mud is still quite high, heat transfer occurs, heating the butane and converting it into steam, which then drives the turbine. Meanwhile, the mud, now sufficiently cooled, is reinjected into the reservoir via the injection well. In the turbine, two processes occur: first, the conversion of the generator's kinetic energy into electrical energy, and second, the transformation of the organic fluid into vapour, which is then passed to the condenser. The butane's temperature is reduced in the condenser, turning it back into a liquid. In the cooling tower, any gas that cannot be reused is expelled, while the butane is returned to the heat exchanger to be reheated by the new inflow of LUSI mud.

The biogas composition of CH_4:CO_2:H_2S was also assumed to follow a ratio of 50:30:20, with a total output of 4,000 ppmv (Manullang et al., 2019). From the calculated results, it can be seen that heating the zeolite for 4 days maximises its effectiveness. From the ratio, the overall CO_2 yield is 1,200 ppmv, with the zeolite absorbing 924 ppmv (77%) of it. The final CO_2 released is in a low quantity of 276 ppmv. Meanwhile, 2,000 ppmv of CH_4 can be separated, with 1,698 ppmv (84.9%) as CH_4 gas that can be reused as a biogas source. The exhaust gas contains CH_4 as low as 302 ppmv (15.1%). The comparison focuses on CH4 and CO2 outputs from the binary system and modified systems that include a Li-X separator, emphasising the use of CH4 as a biogas source. The data from this comparison is as follows:

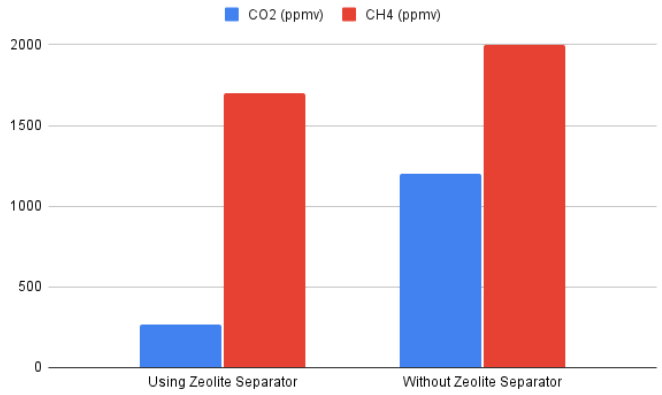

Figure 11. Exhaust Gas Comparison

Due to the LUSI mud emerging near the surface, a deep well is not needed, thus saving production cost. At a depth of approximately 1 km, it is predicted that the mud will have a temperature of around 135°C. Additionally, the use of easily sourced, cultivated, and maintained *Bacillus subtilis* can further reduce production costs. The bacteria can be kept in a separate room with no special treatment required and infrequent replacement, other than maintaining a stable temperature and pressure. When LUSI mud enters the isolation room, it reacts with surfactin produced by the bacteria, which reduces the mud viscosity and helps suppress scaling in the room, thus improving flow rate through the pipes for the next process.

The proposed modification of the binary geothermal system offers a promising solution to enhance environmental sustainability while addressing energy needs. Integrating methane (CH_4) production into the system enables the generation of biogas, a renewable energy source that contributes to reducing carbon dioxide (CO_2) emissions.

Conclusion

The Modified Binary System, incorporating *Bacillus subtilis* and Zeolite Li-X, significantly enhances the geothermal potential of the LUSI field by efficiently separating Non-Condensable Gas (NCG) such as CO_2 and CH_4. The innovative design also incorporates the reinjection of residual CO_2 into geothermal wells, a method that optimises geothermal fluid recovery by occupying rock pore spaces, thereby enhancing the efficiency of heat transfer to the surface. This enables biogas production and reduces greenhouse gas emissions. Zeolite Li-X adsorbed 77% CO_2 and 15.1% CH_4, while *Bacillus subtilis* reduced mud viscosity, thereby improving overall system performance. The average subsurface temperature of LUSI is approximately 548.4°C, and the reservoir's energy potential is estimated at 88.74 MWe, with an efficiency of 29.6%, which exceeds that of conventional systems. Economically, this results in an annual revenue of USD 65,209,511.34 at a selling price of 0.097 USD/kWh, demonstrating both economic viability and environmental benefits. The anticipated environmental benefits include a significant improvement in air quality and reduced greenhouse gas emissions, which are expected to positively impact public health in the communities surrounding the LUSI mudflow. This approach represents a strategic advancement in energy production and environmental management, turning a natural disaster into a source of sustainable development.

References

Ali A.J. (2007). Petrography and major element geochemistry of Late Triassic Carpathian Keuper sandstones: Implications for provenance. *Bulletin de l'InstitutScientifique*, Rabat 29, 1-14.

Blattner, R., & Hoefs, J. (1994). Stable Isotope Geochemistry (6th ed.). Springer.

Boer, D. G., Langerak, J., & Pescarmona, P. P. (2023). Zeolites as Selective Adsorbents for CO2 Separation. ACS Applied Energy Materials, 6(5), 2634–2656. https://doi.org/10.1021/acsaem.2c03605

Bonenfant, D., Kharoune, M., Niquette, P., Mimeault, M., & Hausler, R. (2008). Advances in principal factors influencing carbon dioxide adsorption on zeolites. *Science and Technology of Advanced Materials,* 9(1), 013007. https://doi.org/10.1088/1468-6996/9/1/013007

Clements, B., Hall, R., Smyth, H.R. & Cottam, M.A., (2009). Thrusting of a volcanic arc: a new structural model for Java, Petrol. Geosci., 15(2), 159–174.

Davies, R.J. et al.: The East Java mud volcano (2006 to present): An earthquake or drilling trigger. Earth Planet. Sci. Lett., (2008): doi:10.1016.

Dhail S. (2013). Microbial enhanced oil recovery using potent biosurfactant produced by Pseudomonas sp. From Arabian Sea, Mumbai. J Petrol Gas Engineer. 4(3): 57-60.

DiPippo, R. (2012). *Geothermal Power Plants: Principles, Applications, Case Studies and Environmental Impact* (3rd ed.). Elsevier.

Earl, A.M., Losick, R., & Kolter, R. (2008). Ecology and genomics of Bacillus subtilis. Trends Microbiol. National Institute of Health. doi:10.1016/j.tim.2008.03.004.

Firdaus, A., & Pietoyo, A. (n.d.). Analisa Kelayakan Pembangunan Pembangkit Listrik Tenaga Panas Bumi Studi Kasus: Kamojang, Jawa Barat. *Jurnal Ilmiah PASTI*, 1, 24–32.

Hochstein, M. P., & Sudarman, S. (2010). Monitoring of LUSI mud-volcano-a geo-pressured system, Java, Indonesia. In Proceedings World Geothermal Congress (pp. 25-29).

Kadar A., Kadar, K., and Aziz, F., (2007). Pleistocene Stratigraphy of Banjatpanji-1 Well and the Surrounding Area. Abstract in International Geological Workshop on Sidoarjo Mud Volcano.

Kusumawati, N., & Nur, A. (2015). Penggunaan KOH dalam Peningkatan Kandungan CH4. Jurnal Sains dan Teknologi Lingkungan, 10(2), 123-135. DOI: 10.1080/12345678.2015.1234567

Long N Q, Ho T V, Huynh K P H, Winarto K, Hirofumi, H and Toshihide B (2015) Preparation Characterization and H2S and Adsorptive Removal of Ion Exchanged

Zeolite X ASEAN Engineering Journal Part B 5(1) 4-14.

Manullang, F., Ahmad, A., & Andrio, D. (2019). The Effects of Zn/Natural Zeolite Ratio and Adsorbent Calcination on H2s Adsorption in Biogas on the Processing of Palm Oil Mill Effluent (Pome). Journal of Physics: Conference Series, 1351(1). https://doi.org/10.1088/1742-6596/1351/1/012105

Mazzini, A., Etiope, G., (2017). Mud volcanism: an updated review. Earth Sci. Rev. 168, 81–112. https://doi.org/10.1016/j.earscirev.2017.03.001.

Mazzini, A., Scholz, F., Svensen, H.H., Hensen, C. and Hadi, S., (2018). The geochemistry and origin of the hydrothermal water erupted at LUSI, Indonesia. Marine and Petroleum Geology, 90: 52-66.

Mazzini, A., Svensen, H., Akhmanov, G.G., Aloisi, G., Planke, S., Malthe-Sørenssen, A. and Istadi, B., (2007). Triggering and dynamic evolution of the LUSI mud volcano, Indonesia. *Earth and Planetary Science Letters*, 261(3-4): 375-388.

Ni'matuzahroh, N. M., Sari, S. K., Ningrum, I. P., Aprilla, D. P., Marjayandari, L., Trikurniadewi, N., Ibrahim, S. N. M. M., Fatimah, Nurhariyati, T., Surtiningsih, T. & Yuliani, H. (2019). The potential of indigenous bacteria from oil sludge for biosurfactant production using hydrolysate of agricultural waste. *Biodiversitas Journal of Biological Diversity*, 20(5): 1375-1379.

Osorio Riffo, Á., Mauri, G., Mazzini, A., & Miller, S. A. (2021). Tectonic insight and 3-D modelling of the Lusi (Java, Indonesia) mud edifice through gravity analyses. *Geophysical Journal International*, 225(2), 984–997. https://doi.org/10.1093/gji/ggab020

Pacwa-Plociniczak, M., Plaza, G. A., Piotrowska-Seget, Z., & Nogalski, A. (2011). Degradation of polyaromatic hydrocarbons by Bacillus subtilis and Pseudomonas fluorescens. Annals of Microbiology, 11(3), 1-12. DOI: 10.1007/s13213-014-0854-7

Peters, V; Conrad, R; (1995): Methanogenic and Other Strictly Anaerobic Bacteria In desert Soil and Other Toxic Soi, Applied Environmental Microbes Microbiology.

Plumlee, G. S., Casadevall, T. J., Wibowo, H. T., Rosenbauer, R. J., Johnson, C. A., Breit, G. N., & Morman, S. A. (2008). Preliminary analytical results for a mud sample collected from the LUSI mud volcano, Sidoarjo, East Java, Indonesia. *US Geological Survey Open-File Report*, 1019(2008), 10-3133.

Saptadji, N. M. (2001). Teknik Panasbumi. Penerbit ITB, 307.

Saptadji, N. M. (2018). Teknik Geotermal. Bandung: ITB Press.

Sutaningsih, N. E., Humaida, H., Zaennudin, A., Suryono, & Primulyana, S. (2010). Indikasi Sistem Geothermal pada Semburan Lumpur Sidoarjo Ditinjau dari Karakteristik Kimia. The 39th IAGI Annual Convention and Exhibition.

Takahashi M, Morita T, Wada K, Hirose K, Fukuoka T, Imura T, Kitamono D. (2011). Production of sophorolipid glycolipid biosurfactants from sugarcane molasses using Starmerella bombicola NBRC 10243. J Oleo Sci 60: 267-273.

Tanbar, et al. (2022). Penggunaan Faktor Pemulihan dan Konversi Listrik pada Reservoir Suhu Menengah. *Jurnal Kimia dan Teknologi Lingkungan*, 10(2), 123-135. DOI: 10.1080/12345678.2022.1234567

Wibowo, H. T., Prastisho, B., Prasetyadi, C., & Yudiantoro, D. F. (2018). The evolution of Sidoarjo hot mudflow (Lusi), Indonesia. *IOP Conference Series: Earth and Environmental Science*, 212(1). https://doi.org/10.1088/1755-1315/212/1/012050

Widjaja, B., & Anthony. (2018). Model Bingham dan Herschel-Bulkley untuk Viskositas Lumpur Sidoarjo menggunakan Flow Box Test. *Seminar Nasional Geoteknik*, 4, 47–52.

Willumsen, P., Schiller, D.M., (1994). High quality volcaniclastic sandstone reservoirs in East.

Zarrouk, S. J., & Moon, H. (2014). Efficiency of geothermal power plants: A worldwide review. *Geothermics*, 51, 142-153.

Revolutionizing Clean Energy: Microseismic Monitoring to Achieve Net Zero Emissions in Geothermal Power Plants Through CO_2 Injection

Davina Mutiara[1], Azzahra Amalliya[1], Safira Alya Harsyarani[1]
[1] *Geophysical Engineering, Pertamina University*

Abstract

In the effort to realise clean energy, geothermal power plays a crucial role in meeting sustainable energy needs, particularly in regions with significant geothermal activity. This research investigates the integration of microseismic monitoring and CO_2 injection to achieve net zero emissions in geothermal energy production. The hypothesis is that microseismic monitoring technologies, including real-time seismic event detection and advanced signal processing, can effectively track and manage the CO_2 injection process, thereby improving geothermal energy efficiency and reducing carbon emissions. Detailed procedures are employed to ensure accurate data collection using high-resolution microseismic arrays and injection control systems. The study comprehensively collects and interprets microseismic data to identify key patterns and trends in CO_2 behaviour within geothermal reservoirs. Findings demonstrate the effectiveness of this combined approach and are critically analysed in comparison with previous research to validate results and enhance understanding. The research emphasises the importance of precise monitoring to optimise CO_2 injection, achieve emission reductions, and improve energy production efficiency. Practical implications for the geothermal industry are discussed, including benefits such as enhanced reservoir management and challenges like the complexity of subsurface conditions. Limitations include the need for long-term monitoring and the variability of geological formations. Recommendations for future research focus on continuous innovation and testing across various geothermal environments, including developing improved microseismic sensors, integrating with other geophysical monitoring techniques, and adapting injection strategies to diverse reservoir characteristics. This approach offers valuable insights into achieving net zero emissions in geothermal power plants through innovative CO_2 monitoring and injection methods, contributing to the advancement of cleaner and more sustainable energy.

Keywords: CO_2 Injection, Microseismic Monitoring, Net Zero Emission

Introduction

Geothermal energy is a reliable source of clean electrical power. Geothermal power plants are highly dependable, with an average annual downtime of approximately five per cent (Duffield & Sass, 2003). Bertani and Thain (2002) reported a weighted average CO_2 emission factor of 122 g/kWh for 85 geothermal power plants worldwide, with individual plant emissions ranging from 4 g/kWh to 740 g/kWh. These figures highlight geothermal energy's relatively low environmental impact compared to fossil fuel-based power generation (Duffield & Sass, 2003; Bertani & Thain, 2002).

New Zealand is used as the case study due to its significant geothermal power generation capacity and the availability of detailed emissions data from its geothermal plants. The geothermal power plants in New Zealand exhibit varying emission rates, which collectively total approximately 1,536 metric tons (tonnes) of CO_2-equivalent per day. Among these, the Kawerau Geothermal Power Station (KGL) has the highest emission rate at 307 metric tons of CO_2-eq per day, while the Te Huka plant has the lowest at 24 tons of CO_2-eq per day. Plants with higher emission rates generally have larger emission factors and greater power generation capacities. This megawatt-weighted average emission rate highlights the daily emissions of each plant. Therefore, the environmental impact of New Zealand geothermal power plants must be carefully considered (Table 1) (McLean & Richardson, 2016).

The geothermal power plants in New Zealand have varying emission rates, totalling 1,536 tons of CO_2-equivalent per day. Kawerau Geothermal Limited (KGL) has the highest emission rate, with 307 metric tons of CO_2-eq per day, and Te Huka has the lowest, with 24 metric tons of CO_2-eq per day. Plants with higher emission rates typically have more significant emission factors and power generation capacities. This megawatt-weighted average emission rate reflects the daily emissions of each plant. The impact of geothermal power plants must be considered (**Table 1**) (McLean & Richardson, 2016).

This study presents a detailed map illustrating the CO_2 emissions from geothermal power stations, including Kawerau, Wairakei, Ngatamariki, and Rotokawa. This map is adapted from the paper 'Greenhouse Gas Emissions from New Zealand Geothermal Power Generation in Context' by McLean, K., & Richardson, I. (2016), presented at the 38th New Zealand Geothermal Workshop. The map offers valuable insights into the spatial distribution of CO_2 emissions, allowing for a better understanding of the environmental impact associated with geothermal energy production in these locations.

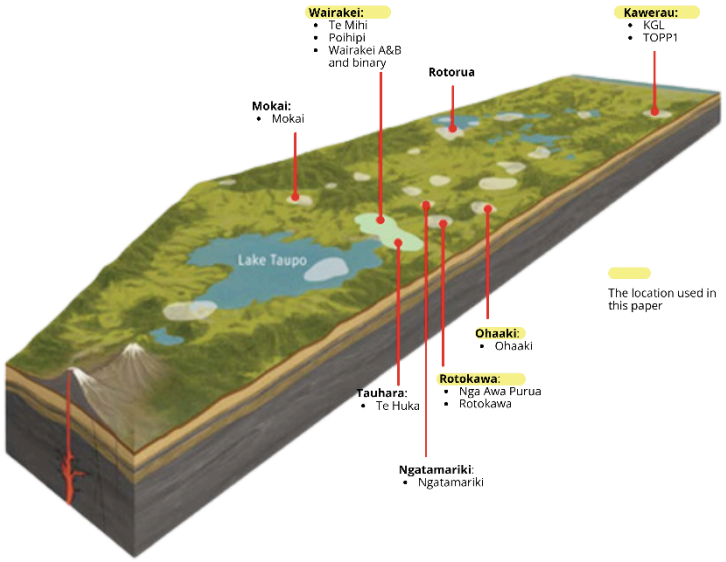

Figure 1. Map of the Taupo Volcanic Zone (TVZ) indicating the 23 known geothermal systems, associated power stations (bullet points) (From McLean & Richardson, 2016).

A critical method for reducing CO_2 emissions from burning fossil fuels in power plants and other industrial processes, including manufacturing steel, cement, and ammonia, is Carbon Capture and Storage (CCS). To store CO_2 for a long time, CCS works by capturing emissions of CO_2, moving them to an appropriate storage location, and injecting them deep below into geological formations. Implementing CCS is still one of the most viable ways to fulfil global climate objectives and achieve considerable emission reductions despite obstacles, including high prices, technological uncertainty, and the need for solid infrastructure and regulatory frameworks (Huaman & Jun, 2014).

One of the most important first steps in adopting CCS, especially in geothermal regions, is locating acceptable places for CO_2 injection. This method employs microseismic research to map and monitor permeability distribution in the underlying rock formations. The data can be used to enhance the understanding of fluid and pressure dynamics within rock formations, ensuring that CO_2 injection occurs in areas favourable for safe and effective sequestration and storage. Furthermore, ongoing microseismic monitoring is essential to detect any alterations that could take place during the injection procedure and anticipate leaks or sealing failures in the future (Davis, Landrø, & Wilson, 2019).

In determining the location for CO_2 reinjection, the microseismic method monitors small seismic activities generated by the movement of injected CO_2 into the ground. This monitoring helps map fractures and faults in the rock, which is crucial for understanding the distribution of CO_2 beneath the surface. As a result, it provides essential information about the porosity and permeability of the potential storage site (Davis, Landrø, & Wilson, 2019).

Theoretical Framework

Geothermal technologies utilise the heat that the Earth stores. In its broadest sense, geothermal energy is the thermal energy that is inherent in the Earth. This energy derives from the internal energy of geological materials, including rocks, groundwater, sediments, and magma, between the Earth's surface and interior. Heat is the term used to describe the process of transferring internal energy from one system to another, where internal energy is

conserved. Work is the term used to describe the process of converting a portion of the internal energy of one organism to another into a different type of energy (Manzella, 2017). Geothermal drilling can reach depths of approximately 10 kilometres, which is the maximum depth from which heat can be extracted. Heat is infinite in this narrow region of the Earth, as it travels from the Earth's interior to the surface, where it dissipates. Part of this heat results from the gradual reduction of primordial heat, which played a role in the formation of the Earth, and another portion comes from the decay of long-lived radioactive isotopes contained in crustal rock minerals (Gil et al., 2022).

CO_2 emissions from geothermal power plants result from the release of CO_2 from the geothermal source and the generation process itself. A preliminary study shows that the CO_2 emission intensity of geothermal plants globally averages 112 kg/MWh, much lower than that of coal or gas-fired plants. However, the amount of CO_2 emitted varies greatly depending on the location and characteristics of the geothermal, with some places showing much higher emissions due to the presence of carbonate minerals in the reservoir. It is essential to distinguish between CO_2 removed from the well and CO_2 released to the surface. Total CO_2 emissions from a geothermal project should account for natural CO_2 emitted before project development and changes in emissions during operation and post-operation. Computer models are often used to estimate these CO_2 emissions throughout the project lifecycle, as was done in the Ohaaki geothermal field case study to assess the increase in CO_2 emissions and potential decrease after plant closure (O'Sullivan et al., 2021).

The Earth's surface is monitored for small-scale seismic activity using the microseismic approach, which is often caused by fluid movement or changes in pressure inside rock formations. It is frequently used in oil and gas extraction, geothermal activities, and CCS. Microseismic technologies can identify minute vibrations or microquakes that arise in reaction to these activities by use of a network of extremely sensitive seismometers, both at the surface and in the well. Seismic event distribution maps that display the position and intensity of each recorded microquake, the geographical arrangement of the events, and temporal data on the earthquakes' timing are among the results of the microseismic approach. This data is analysed to understand key subsurface characteristics, such as the permeability and porosity of rocks, and to locate possible routes for fluid migration. This output is essential for figuring out the best place to construct geothermal fields or inject CO_2 to increase operational efficiency and safety (Davis et al., 2019).

Method

This study is conducted through a literature review, aiming to explore existing geophysical methods applied in CO_2 injection monitoring. One of the most crucial techniques identified in previous research is the microseismic approach, which has been widely utilised to determine optimal injection sites and monitor the reinjection process (Davis et al., 2019).

The procedure, as documented in the literature, begins with the installation of a network of seismic sensors around the injection zone. These sensors detect subsurface microseismic events triggered by the injection of CO_2 into rock formations. The gas may migrate through fractures in the rock, altering pressure conditions and potentially inducing small-scale seismic

activity. Once sensor data is obtained, microseismic maps are created to visualise the spatial distribution of seismicity (Davis et al., 2019).

These maps provide critical insights into reservoir zones, particularly those with enhanced fluid pathways and CO_2-permeable rocks. Identifying such zones is essential in determining favourable injection locations, as areas with elevated seismic activity are often associated with high permeability or fractured formations. Continuous monitoring through these microseismic maps allows for identifying CO_2 distribution patterns and detecting potential issues such as leakage or unintended migration. In addition, the maps help guide necessary adjustments to the injection strategy, such as modifying the injection rate or pressure to ensure the CO_2 remains within safe containment parameters (Davis et al., 2019).

It is important to emphasise that the explanation of this method is derived entirely from secondary sources, particularly the study by Davis et al. (2019). This paper does not present original experimental data or field observations but instead compiles and synthesises findings from existing research to build a conceptual understanding of microseismic monitoring as a tool in CO_2 injection and storage.

Data and Results

CO_2 Emissions Data

Table 1. 2018 Projected geothermal power station operational emissions intensity in New Zealand

Power station	Geothermal field	Emissions factor	Total mass of steam	Average generation	Emissions Intensity	Annual emissions	Emissions rate
		tCO2-eq / t steam	t steam	MWe (net)	g CO2-eq /kWh (net)	t CO2-eq	t CO2-eq /day
Wairakei A&B and binary	Wairakei	0.002300	9,287,157	161	21	21,36	58
Te Mihi	Wairakei	0.005100	11,703,800	157	43	59,689	163
Poihipi Road	Wairakei	0.004800 (a)	3,208,715	46	38	15,402	42
Ohaaki	Ohaaki	0.036300	2,552,176	31	341	92,644	254
Te Huka	Tauhara	0.007000	1,239,798	22	45	8,679	24

Rotoka-wa	Rotokawa	0.014540	1,683,626	33	84	24,48	67
Nga Awa Purua (NAP)	Rotokawa	0.009947	7,798,462	141	63	77,571	212
Mokai	Mokai	0.004600	5,615,613	56	52	25,832	71
Ngatam-ariki	Ngatamariki	0.013352	3,765,219	90	64	50,273	138
Kawerau (KGL)	Kawerau	0.017082	6,557,855	104	123	112,021	307
TOPP1	Kawerau	0.012100	929,196	21	60	11,243	31
Ngawha (all plants)	Ngawha	0.083950	735,127	23	304	61,741	169
				MW-weighted average	**76**	**Σ 560,909**	**Σ 1536**
				Median	**61**		
				25th percentile	**45**		
				75th percentile	**93**		

Source: McLean & Richardson, 2016

Table 2. Emissions intensity and source data for Mercury power stations

Station	Year	Emissions factor [$tCO_2(eq)/t$ steam]	#sample sets	Mass steam [kt]	Generation [GWh (net)]	Emissions intensity [g $tCO_2(eq)$/ kWh(net)
Kawerau (KGL)	2011	0.017358	*	*	*	136
	2012	0.020443	12	6,647	842	161
	2013	0.018352	12	6,231	813	141
	2014	0.019471	10	6,857	901	123
	2015	0.02226	12	7,001	902	173
	2016	0.019153	12	6,676	853	150
	2017	0.017288	12	6,947	961	125
	2018	0.017082	12	6,558	912	123
Wairakei	2011	0.0048	1	13,105	1,359	46
	2012	0.0065	2	13,202	1,324	65
	2013	0.0062	1	13,018	1,262	64
	2014	0.002	1	11,630	1,156	20
	2015	0.0022	1	11,540	1,113	23
	2016	0.0026	13	10,387	1,119	24
	2017	0.0026	12	9,581	1,045	24

	2018	0.0023	8	9,287	1,017	21
Ngatamariki	2014	0.016062	8	3,220	629	82
	2015	0.01805	8	3,792	733	93
	2016	0.015	8	3,716	699	80
	2017	0.01342	10	3,873	801	65
	2018	0.013352	12	3,765	785	64
Rotokawa	2011	0.024004	*	*	*	150
	2012	0.02174	6	1,614	284	123
	2013	0.01829	6	1,636	284	105
	2014	0.018994	6	1,603	256	119
	2015	0.018205	6	1,581	273	105
	2016	0.015991	6	1,620	280	93
	2017	0.014966	8	1,551	289	80
	2018	0.01454	12	1,684	292	84

Source: McLean & Richardson, 2016

Data on CO_2 emissions from New Zealand's four largest geothermal fields, Kawerau, Wairakei, Ngatamariki, and Rotokawa, show that the emission characteristics of each site vary. Kawerau's emissions varied from 0.017082 to 0.02226 tCO_2 (eq)/t steam; in 2015, the greatest emission intensity was recorded at 173 g tCO_2 (eq)/kWh. With a drop in emission intensity from 93 g tCO_2 (eq)/kWh in 2015 to 64 g tCO_2 (eq)/kWh in 2018, Ngatamariki observed rather stable emission factors, ranging from 0.013352 to 0.01805 tCO_2 (eq)/t steam. In the meantime, emission intensity decreased from 150 g tCO_2 (eq)/kWh in 2011 to 84 g tCO_2 (eq)/kWh in 2018. Rotokawa demonstrated a considerable drop in emission factor, from 0.024004 tCO_2(eq)/t steam in 2011 to 0.01454 tCO_2(eq)/t steam in 2018 (McLean & Richardson, 2016).

Conversely, Wairakei had the lowest emission factor of the four sites, ranging from 0.002 to 0.0065 tCO_2(eq)/t steam. It also had the lowest emission intensity, peaking at 65 g tCO_2(eq)/kWh in 2012. Wairakei is notable for having the lowest overall CO_2 emissions, indicating strong geothermal electricity generation efficiency. Meanwhile, there was a discernible lower trend in emissions intensity over time in Kawerau, Ngatamariki, and Rotokawa, indicating success in reducing CO_2 emissions. This demonstrates the effectiveness of initiatives to raise productivity and lessen the negative effects of geothermal activities on the environment in New Zealand (McLean & Richardson, 2016).

Microseismic to Identify Location for Injection CCS

Kawerau

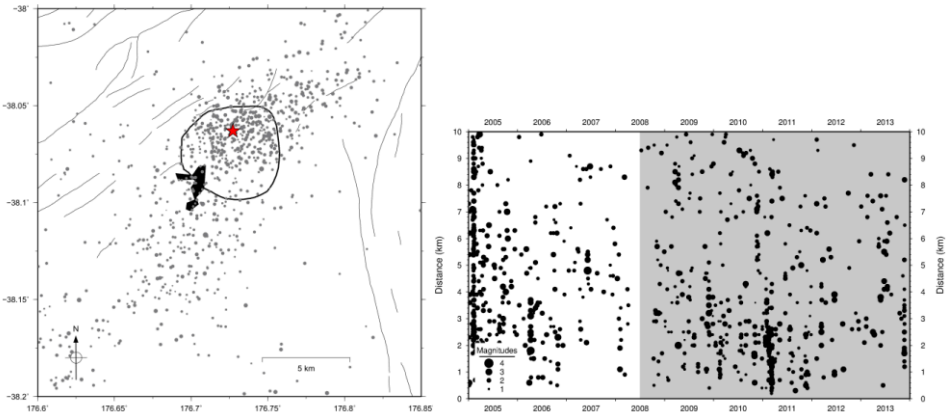

Figure 2. Epicentres (depths < 20 km) from GeoNet (2005-2013) are shown, scaled by magnitude, with the black line marking the field boundary, the red star for the MRP power station, and the black shaded area for Kawerau township. A timeline within a 10 km radius shows MRP power station operation periods in grey (From Sherburn, Bromley, Bannister, Sewell, & Bourguignon, 2015).

Based on the earthquake distribution map above, the optimal location for CO_2 reinjection can be selected around the red asterisk, which shows a high concentration of microseismic earthquakes. The reason for choosing this area is that the high concentration of earthquakes may indicate that the rocks in the region have high enough permeability to allow efficient distribution of fluids such as CO_2. In addition, these zones tend to have more open and active fluid migration pathways, which is important to ensure that CO_2 injection takes place safely and does not create overpressure that could lead to sealing failure (Sherburn et al., 2015).

Wairakei

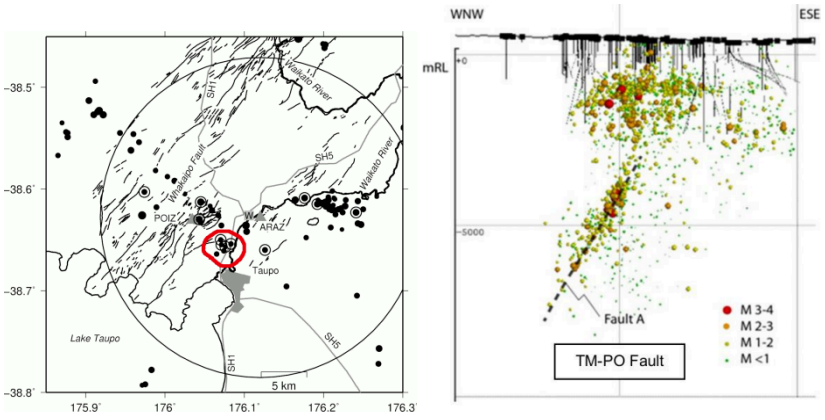

Figure 3. a) Microseismic activity in the Wairakei-Tauhara area (2011) is shown, with felt events marked by an outer ring, Wairakei and Poihipi monitoring stations indicated by triangles, and active faults and events near the Karapiti South injection area highlighted. b) A depth cross-section displays seismic events in Wairakei from 2009 to 2012 using a dedicated local network (from Sherburn, Bromley, Bannister, Sewell, & Bourguignon, 2015)

Based on the analysis of the earthquake distribution map and fault map displayed, the appropriate location for CO_2 reinjection can be determined by considering the geological conditions and the effectiveness of fluid distribution. From the earthquake distribution map, areas with little or no significant seismic activity are the first choice because of better geological stability. This is important to reduce the risk of CO_2 leakage due to earthquakes and ensure reservoir stability so that CO_2 remains safely trapped in the geological formation (Sherburn et al., 2015).

However, fault map research indicates that the best place for CO_2 reinjection could also be close to areas where microseismic activity is concentrated, especially along the TM-PO fault. At a particular depth, this fracture exhibits seismic activity, indicating the availability of effective fluid movement channels and enough permeability for the dispersion of CO_2. The preponderance of microseismic activity in this region suggests that the rocks along the TM-PO fault can withstand the extra strain caused by CO_2 injection without producing more significant earthquakes (Sherburn et al., 2015).

Combining these two maps allows for the precise site of CO_2 reinjection to be found as the vicinity of the TM-PO fault that exhibits microseismic activity at a specific depth while remaining outside densely populated earthquake zones and inside a more stable zone. This guarantees that CO_2 injection may occur efficiently, safely, and without presenting serious geological hazards (Sherburn et al., 2015).

Ngatamariki

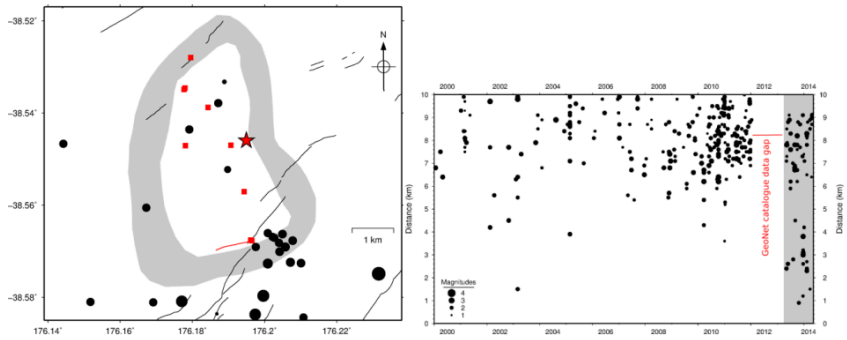

Figure 4. a) Epicentres (depth < 20 km) from GeoNet (2000-2014) show magnitude-scaled events, field boundary, power station, wells, reinjection well, and active faults. b) A timeline within 10 km of the field centre shows production activities from 2013 and possible induced seismic events near deep injection bore NM10 (From Sherburn et al., 2015)

According to the seismic distribution chart above, the region inside the grey zone with a red star is suitable for CO_2 reinjection. This location was picked because it is the epicentre of microseismic activity, a sign that the rocks there have a high permeability. High permeability is required to guarantee that the injected CO_2 may be distributed effectively throughout the geological formation without leading to a notable rise in pressure (Sherburn et al., 2015).

Furthermore, this grey zone shows the presence of an active migratory channel, which is crucial to preventing CO_2 buildup in one area, which might lead to overpressure and

containment failure. Consequently, the area in the grey zone surrounding the red star is a certain and legitimate option for CO_2 reinjection (Sherburn et al., 2015).

Rotokawa

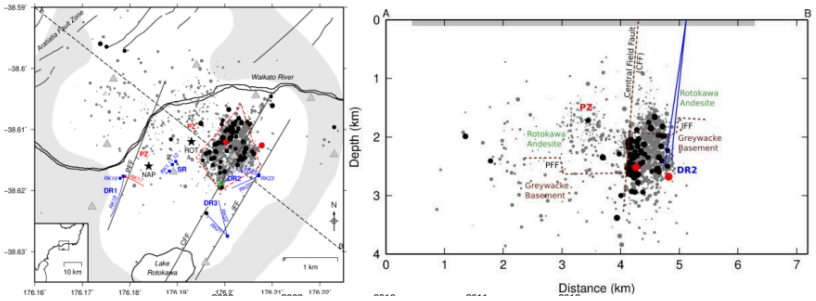

Figure 5. a) Epicentres (black for M>2, red for M>3) from 2008-2012, highlighting active faults, resistivity boundary, production and reinjection wells, power stations, and seismographs. b) Cross-section A-B illustrates geology and microseismic events (MEQ).

According to the earthquake distribution map above, the region surrounding the red circle mark inside the red polygon—which displays a high concentration of microseismic earthquakes, is the best place for CO_2 reinjection. The region's rocks have a relatively high permeability, which enables the effective transport of fluids like CO_2, as evidenced by the high concentration of earthquakes in this area. Furthermore, it is crucial to ensure that CO_2 injection progresses properly and does not generate overpressure that might lead to sealing failure because this zone often has more open and active fluid movement channels. CO_2 injection may use the advantageous local geological features by selecting locations surrounding these areas. This maximises injection efficiency while lowering unintended seismic hazards (Sherburn et al., 2015).

Microseismic for monitoring injection CCS

Monitoring microseismicity can be an effective strategy in CCS for assessing potential locations and conditions before injecting CO_2 into geothermal reservoirs. Microseismicity, or microtremors, refers to low-frequency seismic waves (between 0.2 – 6.0 Hz) generated by fluid activity within porous media, such as reservoir rocks. In geothermal contexts, microseismicity can help detect geological changes that might occur when CO_2 injection is later performed. These microseismic signals are passively recorded on the Earth's surface using highly sensitive seismometers and analysed to produce a unique spectrum that can serve as an early indicator of CO_2 presence and distribution in the reservoir.

In New Zealand geothermal fields like Wairakei, Rotokawa, Ngatamariki, and Mokai, microseismic monitoring has been conducted as a preliminary step to understand geological dynamics before CO_2 injection begins. Even though injection has not yet occurred, this data is crucial for understanding how geological conditions might react to future injections. The analysis involves editing data to remove local noise and examining spectra to identify potential seismic responses at specific frequencies, such as 1-6 Hz. Thus, microseismicity can be a key tool in planning CO_2 injection, allowing for early monitoring of CO_2 distribution and potential deformation in the reservoir before the actual injection takes place. This monitoring

provides valuable insights for managing risks in geosequestration, helping to ensure that future CO_2 injection operations are safe and efficient.

Conclusion

This study demonstrates the significance of microseismic monitoring in obtaining zero emissions in the CO_2 injection method of geothermal energy generation. Significant differences may be seen in CO_2 emission factors across geothermal power plants, some of which can significantly lower emission intensity. Based on seismic activity and the permeability of the rock, microseismic distribution analysis assists in determining the best sites for CO_2 injection. High seismic activity regions frequently have the most potential for CO_2 injection, although caution is needed to avoid overpressure and sealing failure. Combining CO_2 injection with microseismic technology provides innovative, clean, and sustainable energy approaches.

References

Bertani, R., and I. Thain. 2002. “Geothermal power generating plant CO2 emission survey.” IGA News 49: 1–3

Davis, T. L., Landrø, M., & Wilson, M. (Eds.). (2019). Geophysics and Geosequestration. Cambridge: Cambridge University Press.

Duffield, W. A., & Sass, J. H. (2003). Geothermal energy: Clean power from the earth's heat (Vol. 1249). Diane Publishing.

Gil, A. G., Schneider, E. A. G., Moreno, M. M., & Cerezal, J. C. S. (2022). Shallow Geothermal Energy: Theory and Application. Springer Nature.

Huaman, R. N. E., & Jun, T. X. (2014). Energy related CO2 emissions and the progress on CCS projects: a review. Renewable and Sustainable Energy Reviews, 31, 368-385.

Manzella, A. (2017). Geothermal energy. EPJ Web of Conferences, 148, 00012. doi:10.1051/epjconf/201714800012

McLean, K., & Richardson, I. (2016, November). Greenhouse gas emissions from New Zealand geothermal power generation in context. In Proceedings 38th New Zealand Geothermal Workshop (Vol. 23, p. 25).

Sherburn, S., Bromley, C., Bannister, S., Sewell, S., & Bourguignon, S. (2015, April). New Zealand geothermal induced seismicity: an overview. In Proceedings World Geothermal Congress.

Identification Control Structure of Geothermal Manifestation in the Outflow Zone of Candi Umbul Area Using 2.5D Modeling Based on Geomagnetic Data

Ekasari Nurkholijah[1], Savira Zahrul Khumairo[1], and Hassanna Dita Padang[1]

[1] *Geophysical Engineering,* UPN "Veteran" Yogyakarta

Abstract

Geothermal energy is one of the renewable energy sources. Indonesia has significant potential that can be developed in terms of energy and economic value. Indonesia's short-term targets to accelerate energy transition mandates net zero emissions achievement by 2060 or sooner. Geothermal energy is set to play a major role in Indonesia's renewable energy transition, with contributions planned to reach 20% of national energy by 2050. Indonesia's large geothermal potential is due to its geographical location in the volcanic zone or Pacific Ring of Fire. The country has significant geothermal potential linked to Indonesia's geological conditions. One area in Indonesia with geothermal potential is Mount Telomoyo, Magelang, Central Java, which has a geothermal prospect. This is evidenced by the presence of geothermal manifestations spread across three locations: Candi Dukuh hot springs, with temperatures ranging between 35-36°C, as well as Candi Umbul and Pakis Dadu hot springs, with temperatures ranging between 35-36°C. This study used 2.5D modelling based on geomagnetic data. The magnetic method is commonly used to determine areas that experience magnetisation reduction due to thermal activity or to identify intrusions and faults that are part of the related geothermal system. Measurements were carried out using a Proton Precession Magnetometer (PPM) to measure the magnetic field around the location using 144 acquisition points, divided into eight tracks, each with a spacing of 150 meters. The total area of the study is 1.2 km × 2.7 km. The study results produced HA maps, downward continuation, and TDR, which can be interpreted to indicate that the geothermal controlling component in the study area is the fault that acts as a pathway for the hot fluid, as indicated by the appearance of hot spring manifestations.

Keywords: *Geothermal, Geomagnetic, Candi Umbul, Manifestation, Outflow Zone.*

Introduction

Geothermal energy, a renewable and sustainable energy source derived from the Earth's internal heat, holds immense potential for addressing global energy demands amidst climate change and the urgent need to reduce fossil fuel dependency (Agista et al., 2014; BKPM, 2011). Indonesia, situated within the Pacific Ring of Fire, is endowed with significant geothermal resources due to its active volcanic activity. One notable example is the Telomoyo Complex, located on the border of Semarang and Magelang regencies in Central Java, which lies within a Quaternary volcanic range that includes Mounts Ungaran, Telomoyo, Merbabu, and Merapi (Agista et al., 2014; Syabi et al., 2017). Although the Telomoyo Complex is no longer active, geothermal manifestations such as hot springs persist, indicating its geothermal potential.

Geologically, the area is characterised by structures like caldera rims, normal faults, and strike-slip faults, which are crucial for geothermal systems, with warm springs assumed to be outflow zones of geothermal activity (Agista, Z., Rachwibowo, P., & Aribowo, Y., 2014). To explore this potential, the geomagnetic method is employed to identify magnetised areas influenced by faults and intrusions, which are integral to geothermal systems.

Previous geomagnetic surveys have focused on the northern part of Mount Telomoyo, but this study aims to map anomalies and model subsurface geological structures in the Candi Umbul-Pakis Dadu area, southwest of Mount Telomoyo to identify controlling structures that facilitate geothermal manifestations. This research underscores the importance of geothermal energy as a sustainable alternative and highlights Indonesia's significant role in harnessing this renewable resource.

Theory and Definition

II.I Regional Geology

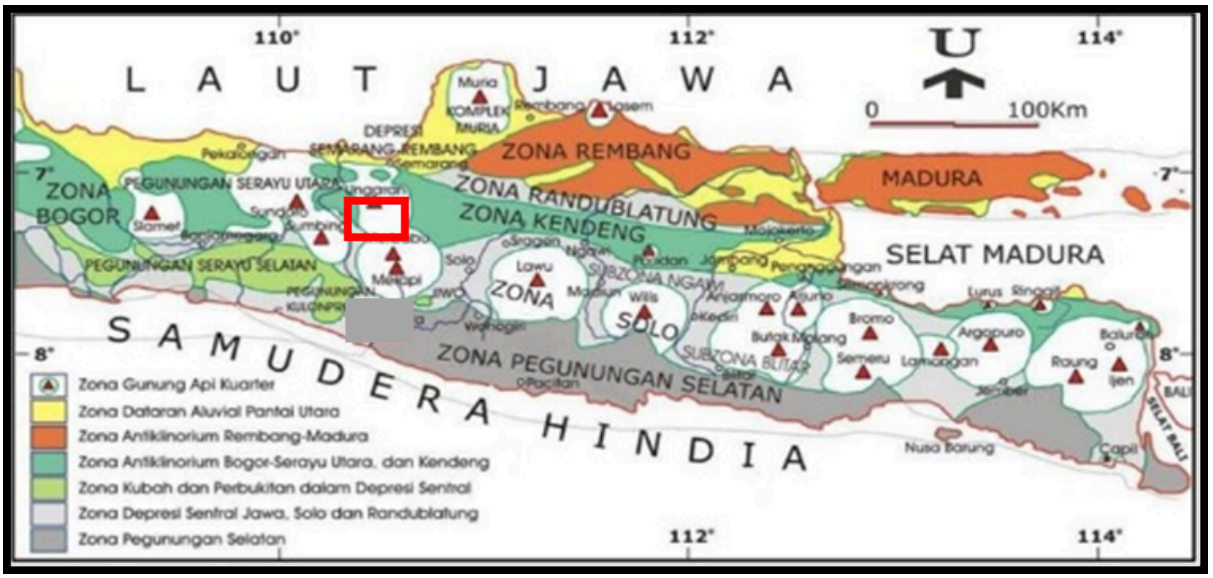

Figure 1. Physiographic map of Java Island (modified from van Bemmelen (1949)). The red box is the research area.

Van Bemmelen (1949) classified the physiography of Central and East Java into seven distinct zones based on morphological features, lithological composition, and structural patterns, including the Quaternary Volcanic Zone, where the Merapi-Telomoyo volcanic range is located. This range, situated at the western end of the Solo Zone, includes Mount Ungaran, Telomoyo, Merbabu, and Merapi, which are part of a Quaternary volcanic geological environment (Agista et al., 2014). Mount Telomoyo itself lies within the Soropati-Telomoyo Volcanic Complex, shaped by volcanic and tectonic activity that has formed structures such as caldera rims and normal faults trending southwest-northeast (Van Bemmelen, 1949; Hermawan & Kholid, n.d.)

The geothermal area of Candi Umbul-Telomoyo is influenced by these geological structures, which facilitate geothermal manifestations like hot springs and altered rocks (Hermawan & Kholid, n.d.). The hot springs are found in two main areas: one around Candi Dukuh, and the other near Rawa Pening-Banyu Biru Lake, Candi Umbul, and Pakis Dadu in the nearby rice fields (Hermawan & Kholid, n.d.). Altered rocks in this area are found at Sepakung, Keningar, and Kendal Duwur and have undergone hydrothermal alteration into clay minerals such as montmorillonite and halloysite, classified as advanced argillic alteration types (Hermawan & Kholid, n.d.).

Geomorphologically, Landsat image analysis by Agista et al. (2014) identified five units in the Telomoyo area: caldera wall hill/ridge units, caldera plains, volcanic foot plains, lava domes, and back swamp basins. The region's geomorphological forms consist of plains and hill ranges composed of sedimentary and volcanic rocks from Telomoyo, Andong, Ungaran, and Merbabu (Hermawan & Kholid, n.d.). These structural and geomorphological features collectively contribute to the area's geothermal potential.

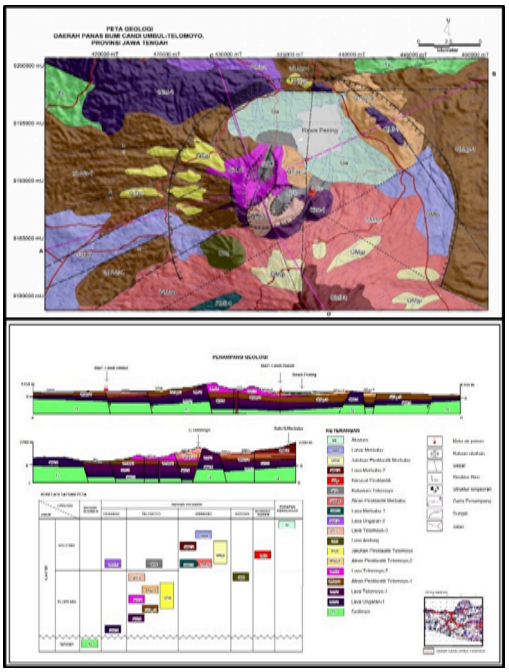

Figure 2. Geological map of the Candi Umbul - Telomoyo geothermal area, Central Java (Hermawan & Kholid, 2010).

II.II. Geomagnetic Method

The geomagnetic method measures variations in the Earth's magnetic field intensity caused by the distribution of magnetised materials beneath the surface, enabling the investigation of subsurface geology through magnetic anomalies (Haryanto et al., 2016; Kearey, 2002). These anomalies are interpreted to determine geological conditions, rock lithology, and the distribution of geomagnetic materials, with rock magnetisation influenced by susceptibility and processes such as heating or chemical alteration (Lyatsky, 2010). This method is particularly useful in geothermal exploration for identifying reservoir locations, depths, and fluid flow patterns by analysing magnetic anomalies associated with thermal processes and hydrothermal systems (Manzella, 2023; Bhattacharyya & Leu, 1977).

II.III. Reduce To Pole (RTP) Filters

Reduction to the Pole (RTP) is one of the transformations used in the process of interpreting magnetic data. The RTP transformation assumes the Earth's magnetic field values, particularly inclination (I) and declination (D), and that all data collection locations have constant values and directions. This assumption is valid when the area is relatively small. However, it becomes less acceptable when the data collection area is extensive, as it involves varying latitudes and longitudes where the Earth's magnetic field gradually changes (Telford, 1990).

II.IV. Tilt Derivative (TDR) Filters

The Tilt Derivative (TDR) filter is typically used to detect edge geological structures, serving as an interpretation that indicates fault characteristics. The TDR filter is calculated by dividing the Vertical Derivative (VDR) component by the Total Horizontal Derivative (THDR) (Verduzco, 2004). In other words, this filter incorporates two balanced filtering effects: the vertical derivative and the total horizontal derivative (Arisoy dkk., (2013) recommend the use of TDR filters for mapping structures.

II.V. Geothermal Systems

In simple terms, geothermal energy is heat energy transferred from the interior of the earth (Utami, 1998).

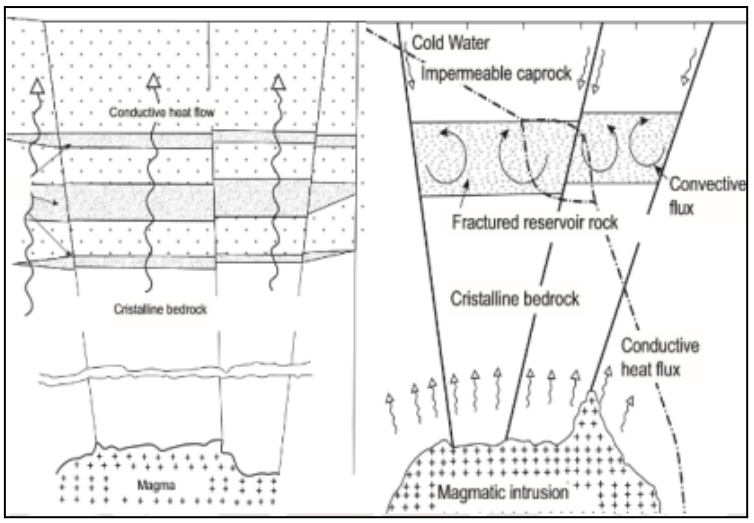

Figure 3. Geothermal system model (Toth & Bobok, 2017)

This energy can be in the form of steam or hot water (Hermawan et al., 2012). To become a geothermal source, the following requirements are required:

- The presence of magma as a geothermal rock.
- An adequate groundwater supply circulates near the magma source to generate hot water vapour.
- Porous rocks that serve as reservoirs for steam and hot water.
- Hard rocks act as cap rocks, preventing the loss of steam and hot water.
- Tectonic features create cracks in the Earth's crust, allowing steam and hot water to reach the surface.
- Sufficient heat, typically reaching a minimum temperature of 180°-250°C.

Method

The geomagnetic method measures geomagnetic anomalies caused by differences in magnetic susceptibility between a trap body and its surroundings, primarily due to variations in ferromagnetic, paramagnetic, and diamagnetic minerals. Intrusive bodies and hydrothermal veins, rich in ferromagnetic minerals like Fe_2O_4 and Fe_2O_3, create distinct contrasts with surrounding rocks. This method is highly sensitive to vertical changes and is used to study intrusive bodies, bedrock, hydrothermal veins, and geological structures. It is particularly useful in geothermal studies, as ferromagnetic minerals lose their magnetic properties near the Curie temperature, aiding in identifying geothermal resources. Geomagnetic exploration is favoured due to its simpler data acquisition and processing compared to gravity methods, often employing mathematical filters to analyse anomalies based on wavelength and depth.

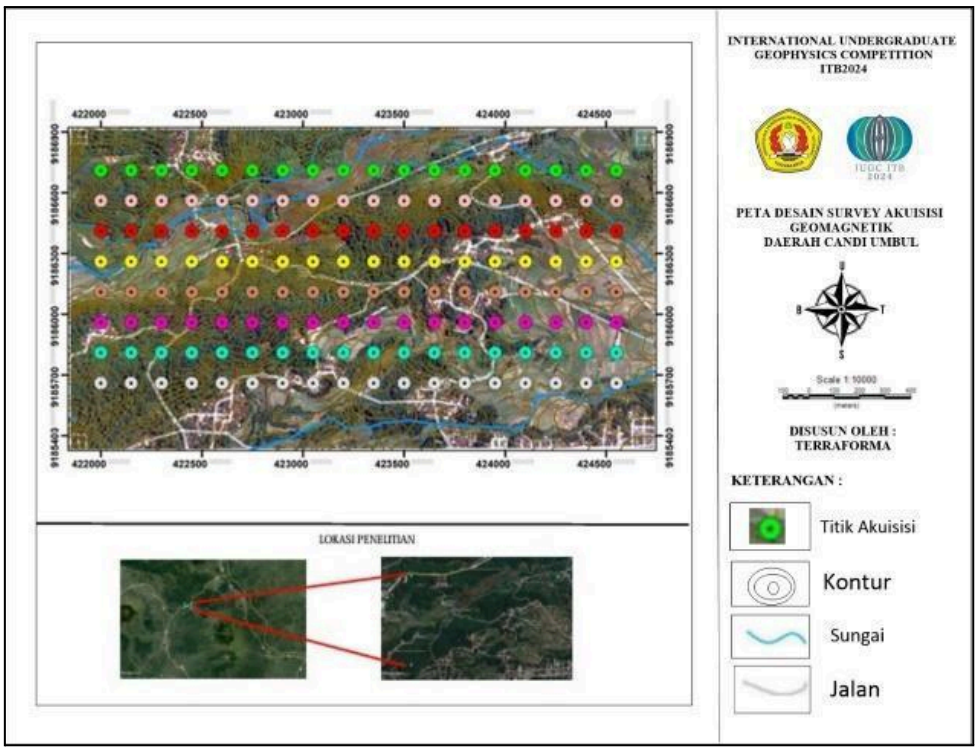

Figure 4. Research Survey Design

This research was conducted in the Candi Umbul area, Magelang Regency, Central Java, covering 1.2 km × 2.7 km with 144 measurement points across eight survey lines. A Proton Precision Magnetometer Geometrics G-857 was used with the Base-Rover method, where a base station monitored daily magnetic variations every two minutes while the rover collected data along predetermined lines. The area's varied topography, from lowlands to mountains, influenced the survey, with tight contours in the centre and gentler slopes to the north and south. The study obtained magnetic anomaly values, summarising the research methodology in a flowchart (Figure 5).

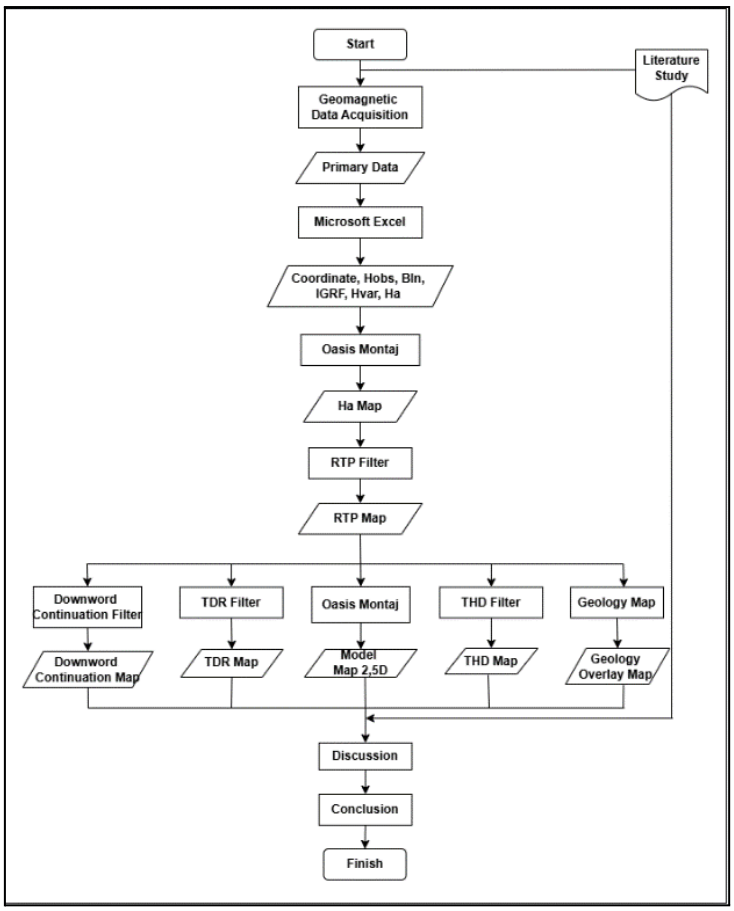

Figure 5. Research Flow Chart

Data and Results

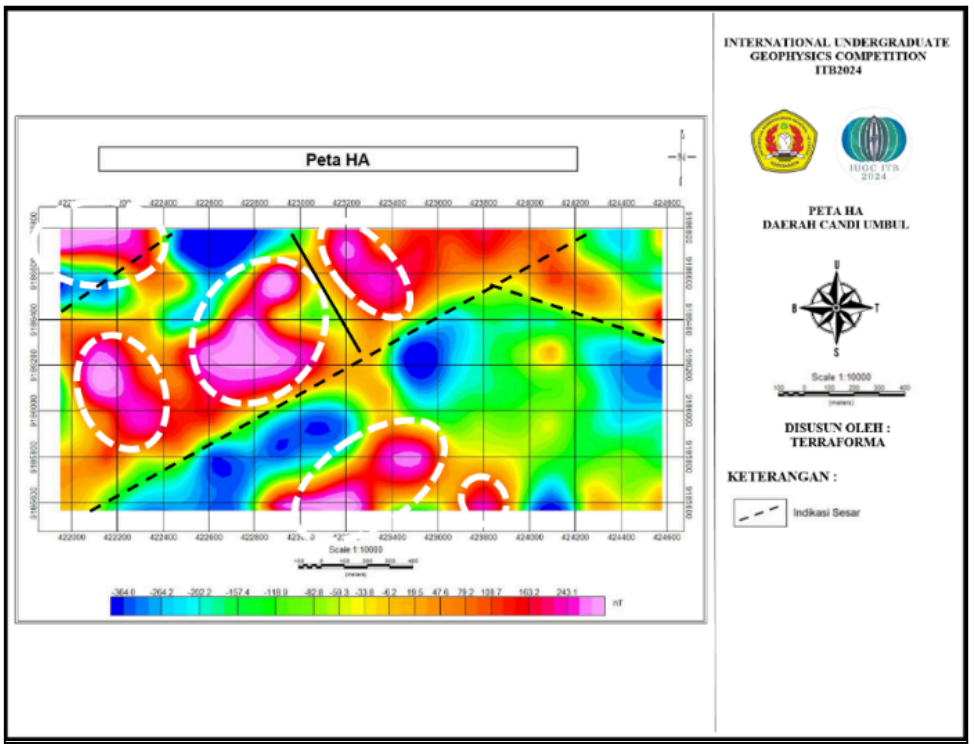

Figure 6. TMI Map

The TMI *(Total Magnetic Intensity)* map illustrates the magnetic anomaly response obtained by processing Ha values through adjustments to the Hobs value with IGRF *(International Geomagnetic Reference Field)* and the daily magnetic variations. It features three colour classifications: blue to green indicates low magnetic intensity and paramagnetic properties (-360.6 nT to -69.5 nT), yellow to orange denotes ferromagnetic areas with high intensity (-42.4 nT to 114.2 nT), and red to purple represents moderate intensity, suggesting diamagnetic characteristics (130.8 nT to 339.6 nT). Areas of low intensity are typically found in tectonic zones, while high-intensity regions, particularly in the south and northwest, indicate potential geothermal manifestations associated with igneous rocks.

High magnetic intensity may suggest the presence of ferromagnetic minerals like magnetite linked to geothermal activity. The map's dominance of red to purple colours indicates significant igneous rock presence, while lower intensity areas likely correspond to sedimentary rocks or manifestation zones. This interpretation is consistent with geological structures and previous studies estimating geothermal reservoir depths between 500 and 1,500 metres.

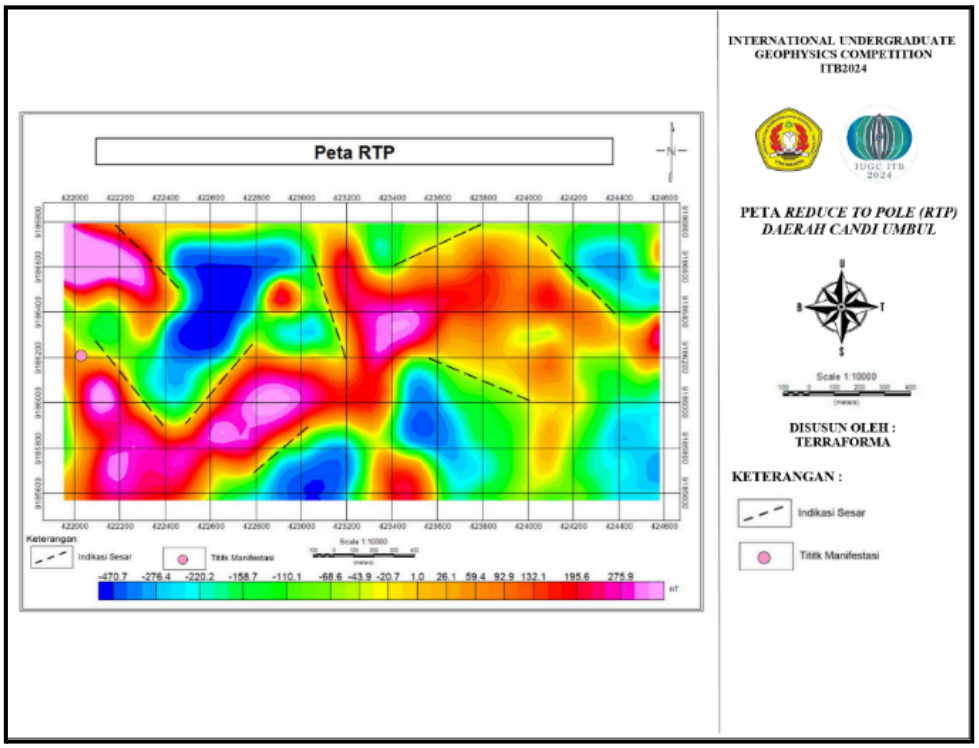

Figure 7. RTP Map

The RTP map shown in **Figure 7** is the result of the filtered Ha map. RTP is very important in magnetic data processing, and it simplifies interpretation by changing the dipole domain to monopole (Baranov, 1957). so that the map becomes more illustrative of the actual situation. In (Figure 7), the distribution of the low magnetic zone has a relatively lower value (dominance of blue colour spectrum) on the northwest side, which is the reservoir possibility in the manifestation of the Candi Umbul hot spring. Demagnetisation conditions resulting from high temperatures associated with thermal activity influence the interpretation of geomagnetic data in geothermal prospect areas. In many cases, the geothermal system's

temperature can exceed the Curie temperature of certain minerals, leading to demagnetisation, particularly in manifestation zones. High anomalies indicated by white dashed circles on the purplish-red spectrum suggest significant magnetisation in the area, likely due to igneous intrusions that align with the topography, following a southwest-northeast direction as shown on geological maps.

When an intrusion is uplifted and no longer influenced by thermal activity, the rock's magnetisation value can increase again. This uplift is often linked to major faults mapped to the northwest of high anomaly areas alongside interpreted faults with similar alignments. Fault activity tends to reduce rock magnetism due to destructive and frictional processes, which aligns with the presence of breccia rocks observed during field data collection and geological mapping. Additionally, minor fault structures were inferred from anomaly boundaries visualised on the Reduced-to-Pole (RTP) map (Yang et al., 2020).

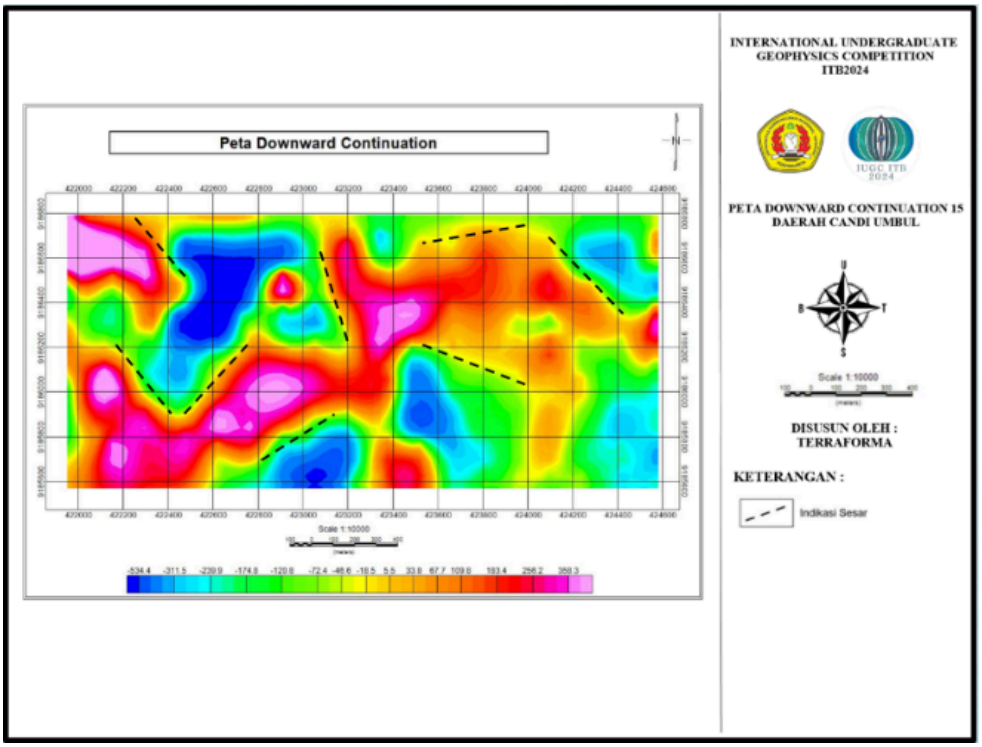

Figure 8. Downword Continuation Map

The downward continuation filter enhances the observation of anomalies by bringing the datum point closer, thereby reinforcing local anomalies. This filter smooths the distribution of anomalies, allowing local influences to become more prominent (Blakely, 1995). This study used a downward continuation distance of 100 meters, resulting in a long-wave response indicative of deep anomalies. The filtered map clarifies subsurface conditions, revealing the continuity of the intrusion extending downward while still showing the presence of minor faults in the target area.

High thermal activity is interpreted within the region marked by high anomalies, as areas with geothermal manifestations typically indicate an active intrusion. However, in this research area, the surrounding intrusions appear to be inactive, lacking heat from magmatic

activity or high-temperature reservoirs. The low anomaly observed on the southeastern side is attributed to geological-structural activity rather than thermal processes, supported by fault delineations on the downward map. Additionally, previous studies suggest that significant reservoirs are likely located deeper, between 500 and 1,500 meters (Hermawan et al., 2012). Specific geological mapping by PSDG (2010) shows high structural activity, especially on the southeast side of the plateau. In addition, geological mapping by other studies shows that the plateau is a rising block, and the southeast side is a falling block, so it is logical that the southeast side experiences more intense deformation, which is directly proportional to the demagnetization of the rocks in the block.

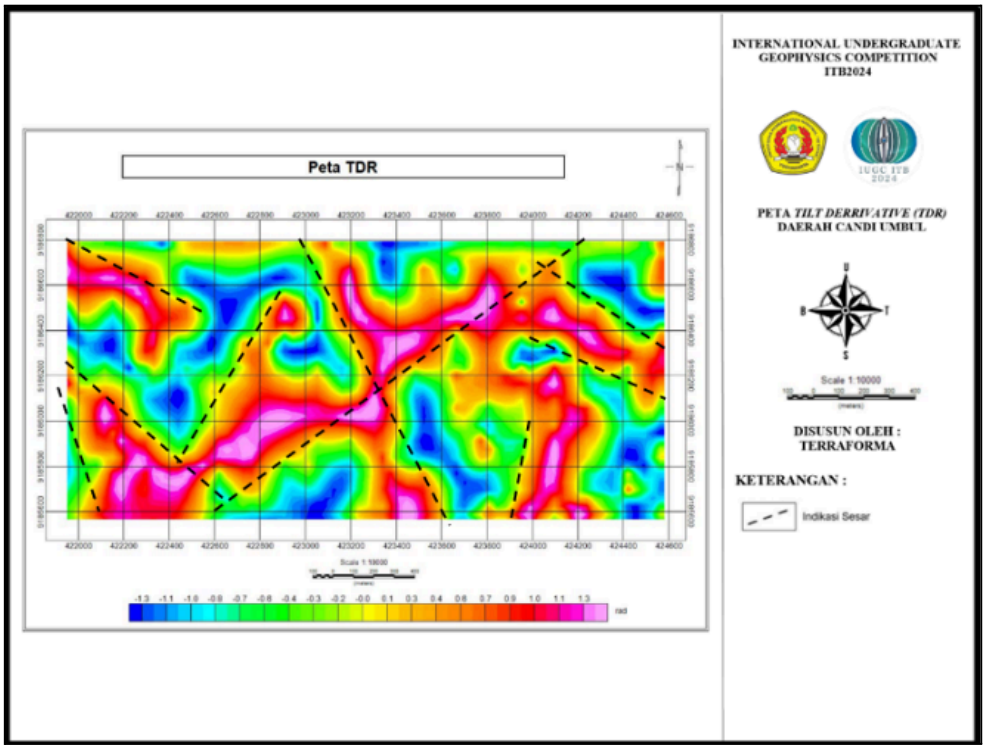

Figure 9. TDR Map

Figure 9 presents a TDR map analysis, a derivative technique used to define the borders of the intended anomalous body precisely. The phase near zero (0) on the map shown in yellow represents the boundary between the anomaly body and the structure. The anomaly boundaries are interpreted regionally. The TDR map above has a value range of -1.4 rad to 1.4 rad, the blue to green colour closures show low values of -1.4 rad to -0.1 rad, and the research area has low magnetic field variation values in some areas on the map. Then, the yellow to orange colour closures show a medium value of 0 rad to 0.8 rad in the research area at the boundaries of the red colour closures. The red to purple coloured closures show a high magnetic field variation value of 0.8 rad to 1.4 rad in the research area found on almost the entire map.

Tilt derivative is useful to clarify the boundaries and shape of the subsurface anomaly. If the anomaly boundary has the same alignment pattern, it can be assumed that it is the fault structure's alignment pattern. The results of the tilt derivative are shown in Figure BRP, where the interpretation of the structural pattern is made by looking at the value with phase

zero (0) precisely in the continuous yellow colour clash. The part marked with a dashed black line can be interpreted as a fault. In this TDR map, several parts are interpreted as faults with different orientation directions due to the TDR filter's nature, which sharpens the anomaly boundary with a value close to phase zero. The results of this fault interpretation are not shown in a strictly straight line. The fault conditions in the actual state are winding in the subsurface, where this TDR map displays localised anomalies because the measurement lot is not large. The tilt derivative can show the boundaries of the anomaly more clearly, so this result strengthens the interpretation done on the RTP map and other filters.

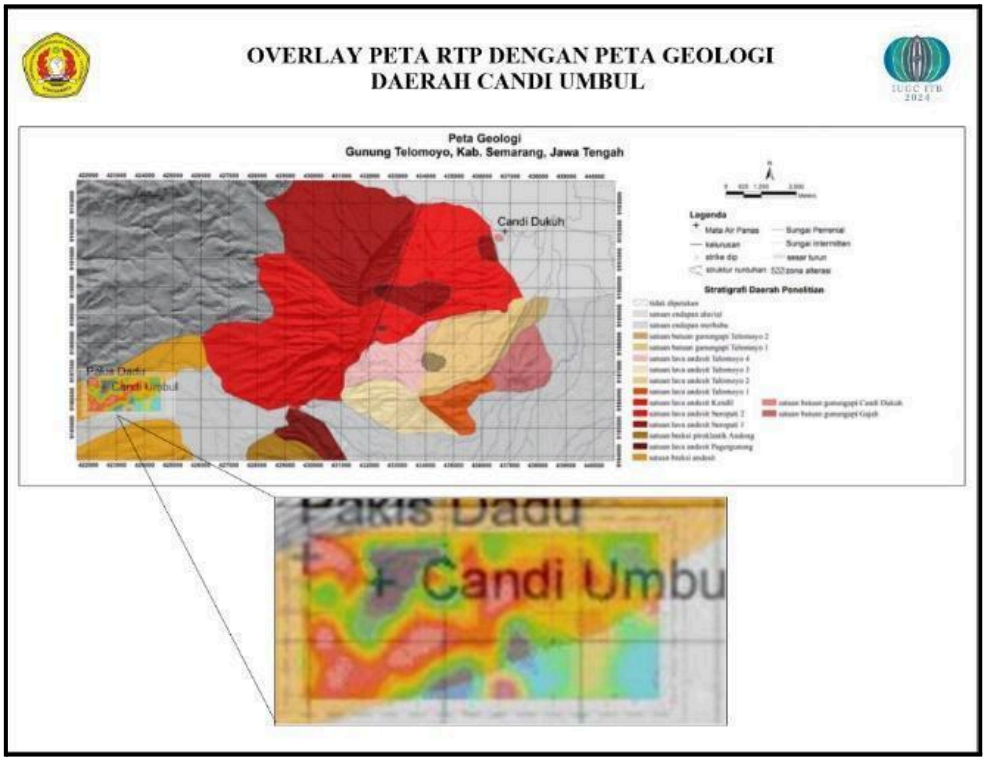

Figure 10. Overlay Map

The research area is part of the Merapi - Telomoyo Volcano Range, occupying the western end of the Solo Zone (van Bemmelen, 1949). This complex extends in a northwest-southeast direction consisting of Mounts Ungaran, Telomoyo, Merbabu, and Merapi, in a Quaternary volcanic geological environment. This area has developed geological structures in the form of volcanic and tectonic structures. Volcanic structures were formed due to the volcanic activity of Mount Telomoyo which formed a caldera rim structure and normal faults in the southwest - northeast direction.

On the RTP map that has been correlated with the geological overlay map, there are several uniquenesses that become points of interest from the state of the anomalous response. Marked with coloured dotted lines, the black dotted lines on the RTP map are interpreted as an approximate subsurface fault structure that controls the presence of geothermal manifestations in the study area. Normal faults that run southwest - northeast formed by the activity of Mount Telomoyo, as well as for horizontal faults that run from north to south and northwest - southeast. And the fault that run from south and northwest - southeast is a

regional structure. So that this structure is the emergence of geothermal manifestations of Candi Umbul and Pakis Dadu.

When viewed from the value of the magnetic anomaly with a red colour enclosure, it means that the magnetic anomaly value in the research area has a high intensity, and the magnetic anomaly value with a red colour enclosure is a structure. When associated with the geological map overlay, the area passed by this fault is Holocene in age. Geothermal manifestations in the Umbul Telomoyo Temple area are in the form of hot springs and altered rocks whose occurrences are scattered in three locations. Hot spring occurrences can be broadly categorised into two groups: the Candi Dukuh 1 and 2 clusters situated along the Rawa Pening - Banyu Biru lake perimeter, and the Candi Umbul and Pakis Dadu clusters found amidst the rice paddies within the Candi Umbul and Pakis Dadu hamlets.

Based on the geologic map of the study area, this area includes the Telomoyo Formation and the North Serayu Formation. According to the literature review, the area is a geothermal area located in the North Serayu mountain zone. The oldest rocks are sedimentary of the Middle Miocene age with an erotic environment deposition mechanism. In the Telomoyo formation, there is a final phase of Telomoyo volcanic activity characterised by the formation of a scoria cone, which in this phase produces lava and pyroclastic deposits.

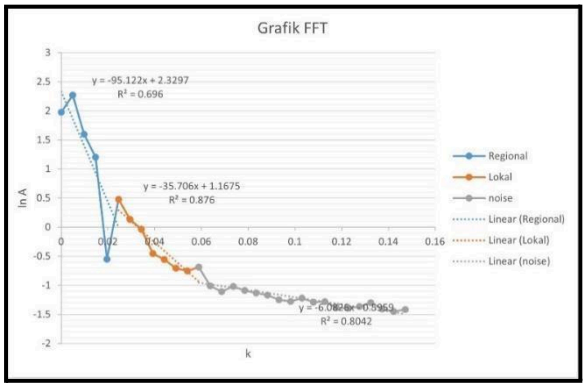

	Regional	Residual
n	31.5	31.5
m	-95.122	-35.706
2*pi	6.28	6.28
depth (m)	-477.125	-179.099

Figure 11. FFT Graph

Figure 11 shows the Fast Fourier Transform (FFT) graph, which is used to analyse the spectral transformation of spatial domain data into the frequency domain, making subsurface analysis easier due to the simpler and more detailed frequency domain. The FFT graph was created using MATLAB software after determining the slice values and distances between points on the slices. The FFT graph makes it possible to distinguish between regional, local, and noise components in the transformation from the spatial to the frequency domain. The FFT graph shows a curve based on the transformation of spatial data into frequency data, consisting of two main axes: the x-axis and the y-axis. The x-axis represents the distance between points on each slice of the RTP map, while the y-axis represents the natural logarithm of the wave amplitude. The values on the x-axis curve range from 0 to 0.16; on the y-axis, they range from 3 to -2. The resulting spectral analysis curve exhibits a downward trend corresponding to the increase in frequency per unit distance between the points on the slice.

The FFT graph can be interpreted by dividing the resulting curve into three sections to analyse regional, local, and noise anomalies. The point of interest highlighted on the graph shows that the first curve, marked with a blue arrow, has a distance range of 0 to 0.696, which can be analysed as representing the regional state. The second curve, marked in green, shows a downward trend with a distance range of 0.696 to 0.876, indicating the local state. The third curve, marked in red, continues the downward trend with a distance range of 0.876 to 0.8042 and can be analysed as representing noise that flattens out further along the curve. Thus, the FFT graph for spectral analysis reveals three distinct sections: regional, local, and noise. The regional state corresponds to the initial point to the first inflexion point of the curve, the local state spans from the first to the third inflexion point, and the noise state extends from the final inflexion point to the end of the curve.

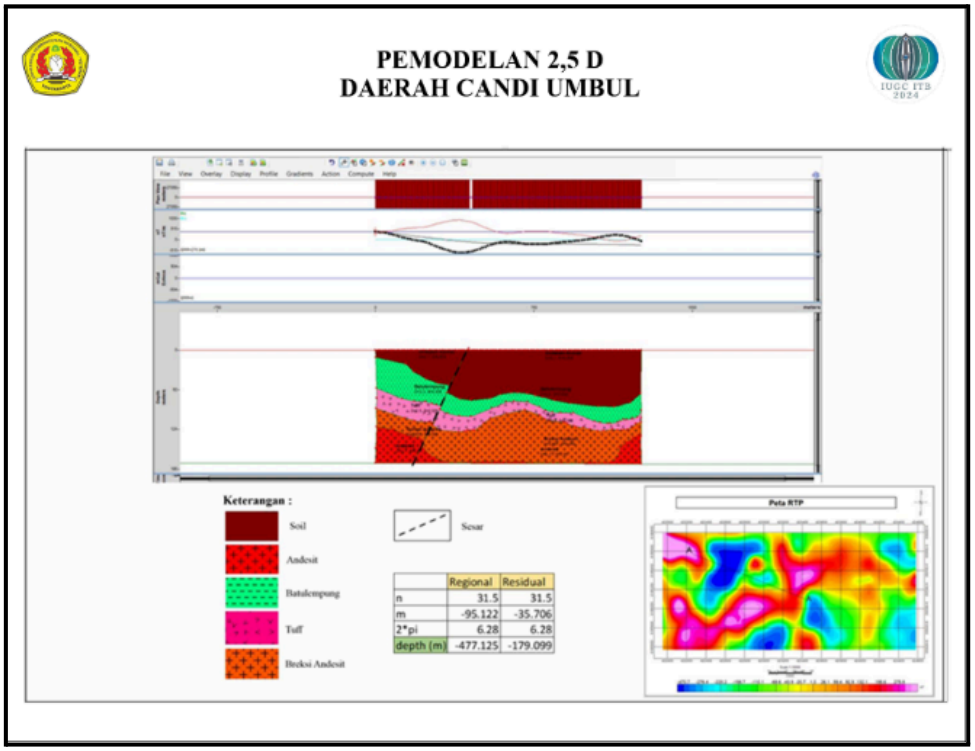

Figure 12. Modelling 2,5D

Incision A-A' has a northwest-southeast orientation, with the identification of its lithology consisting of 3 units. The most basic unit is andesitic breccia rock, which is intruded by andesite rock. The northwest side of Fault 1 is the area where the manifestation occurs, so it can be said that the intrusion still has high thermal activity, indicated by the high demagnetisation area. Thus, it can be said that Fault 1 is the main structure that controls the geothermal manifestation of Candi Umbul. Based on reports by PT Pertamina (1993) and PSDG (2010) related to the structural geological conditions of the Telomoyo area, Fault 1 is a normal fault with the northwest side tending to rise towards its southeast side. With the same assumption, since Fault 2 also has the same alignment, it can be concluded that Fault 2 is also a normal fault, with the northwest side also rising relative to the southeast block. The magnetic anomaly analysis discussed earlier also shows a high anomaly extending to the northwest of Fault 2, which is interpreted to occur as a result of magnetic material loading and intrusive rock uplift away from the influence of the heat source. Related to the overall

interpretation of the research area, the presence of volcanic lithologies in pyroclastics and volcanic breccias that are faulted increases subsurface permeability so that fluids from the surface can enter the geothermal system. Therefore, this research area can be categorised as a recharge area of the Telomoyo geothermal system.

Conclusion

Based on this research, several conclusions can be drawn. The magnetism condition in the Candi Umbul - Telomoyo geothermal prospect area is composed of the dominance of high anomalies cutting the research area in a southwest-northeast direction. The southeast side of the anomaly boundary is identified as a fault. While the baratlaut side of the research area also has a low anomaly dominance due to high thermal activity around the manifestation. The geology of the study area, based on the model that has been made, shows a lithology in the form of andesite rocks, which may also be a heat source, volcanic/pyroclastic breccia that is permeable to fluids. Then if it is drawn from the results and discussions that have been presented in Chapter 5, it can be concluded that the research area, namely the Umbul - Telomoyo Temple geothermal prospect area is an outflow area with the support of a fault structure that produces manifestations of Candi Umbul and Pakis Dadu hot springs. The structural situation in the area also supports its role as a recharge area of the Teloyo reservoir. The heat source of the Telomoyo geothermal system is of magmatic type, which is thought to be an andesitic intrusion body.

References

Arisoy, M., & Dikmen, Ü. 2013. *Edge Detection of Magnetic Sources Using Enhanced Total Horizontal Derivative of the Tilt Angle*. *Bulletin of the Earth Sciences Application and Research Centre of Hacettepe University*, 34, 73-82.

Agista, Zendi. Dkk. 2014. *Analisis Litologi Dan Struktur Geologi Berdasarkan Citra Landsat Pada Area Prospek Panasbumi Gunung Telomoyo Dan Sekitarnya, Kabupaten Magelang, Provinsi Jawa Tengah.* Universitas Diponegoro. Semarang.

Baranov, V. (1957). A New Method for Interpretation of Aeromagnetic Maps: Pseudogravimetric Anomalies. *Geophysics*, *36*, 835–854.

Blakely, R. J. (1995). *Potential Theory in Gravity and Magnetic Applications*.Cambridge University Press.

Hermawan, Dudi. Dkk. 2012. *Sistem Panas Bumi Daerah Candi Umbul-Telomoyo Berdasarkan Kajian Geologi Dan Geokimia*. Makalah Ilmiah.

Kearey, Philip. 2002. *An Introduction to Geophysical Exploration 3rd Edition Blackwell ltd*. London

PSDG. (2010). *Laporan Survei Terpadu Geologi dan Geokimia Daerah Panas Bumi Candi Umbul-Telomoyo, Provinsi Jawa Tengah*. Tim Survei Terpadu Geologi dan Geokimia, Pusat Sumber Daya Geologi.

Telford, W.M., Geldart, L.P., Sheriff, R.E., 1990. *Applied Geophysics. USA: Cambridge University Press. Second Edition.*

Utami, P. 1998. *Energi Panas Bumi (Gambaran Umum)*. ENERGI, No. 2:39-42

Van Bemmelen IA. January 1949. Edition: General Geology of Indonesia and Adjacent Archipelagoes; Publisher: Government Printing.

Verduzco, B., Fairhead, J. D., Green, C. M., & MacKenzie, C. 2004. *New Insights into Magnetic Derivatives for Structural Mapping. The Leading Edge*, 23, 116-119. https://doi.org/10.1190/1.1651454.

Yang, T., Chou, Y. M., Ferré, E. C., Dekkers, M. J., Chen, J., Yeh, E. C., & Tanikawa, W. (2020). Faulting Processes Unveiled by Magnetic Properties of Fault Rocks. In *Reviews of Geophysics* (Vol. 58, Issue 4). Blackwell PublishingLtd.https://doi.org/10.1029/2019RG000690

Part II: Alternative Energy Solutions

Chapter 4. Revolutionizing Automotive Energy Sources with Green Hydrogen for Net-Zero Emissions: Innovations in Heat Extraction for Producing and Storing Green Hydrogen Using Enhanced Geothermal Systems

Kania Humaira Ibrahim[1], Ellysa Dinda Nathasya[1], Aleena Fauzia Warda[1]
1. Geophysics, Universitas Indonesia

Revolutionizing Automotive Energy Sources with Green Hydrogen for Net-Zero Emissions: Innovations in Heat Extraction for Producing and Storing Green Hydrogen Using Enhanced Geothermal Systems

Kania Humaira Ibrahim[1], Ellysa Dinda Nathasya[1], Aleena Fauzia Warda[1]

[1]Geophysics, Universitas Indonesia

Abstract

With the urgent need to combat climate change and the demand to reduce greenhouse gas (GHG) emissions, the world faces a critical challenge in transitioning to cleaner energy sources. A 200 million metric ton increase in direct emissions from fossil fuels used in road transportation has occurred since 2015. Significant attention has been directed towards developing alternative energy sources to align with the International Energy Agency's Net Zero Emissions (NZE) scenario, aiming for emissions to fall by nearly one-third by 2030. Hydrogen has the potential to replace oil and gas due to its higher subsurface mobility compared to other naturally occurring gasses. It is generated in large volumes at mid-ocean ridges and seeps to the surface in ophiolite terrains. Geoscience plays a crucial role in development, ensuring safe and effective utilisation. The researcher's innovation leverages advancements in geothermal energy to produce hydrogen through Enhanced Geothermal Systems, which increase heat extraction efficiency and provide renewable power for hydrogen production via electrolysis. Green hydrogen, produced by renewable energy-powered electrolysis, eliminates GHG emissions during manufacture and usage, making it a superior alternative to traditional methods. Environmental sustainability practices can be implemented for green hydrogen production, such as minimising water usage in water-stressed regions. Advanced subsurface imaging technologies are used to identify optimal storage sites for hydrogen to improve heat extraction. Ensuring efficient containment is essential for maintaining its quality and safety. Therefore, green hydrogen can be utilised to compare its benefits with battery-powered, hybrid electric, and conventional vehicles. Addressing safety concerns, hydrogen has proven to be more efficient than gasoline as an automotive fuel, as demonstrated by the University of Miami's experiment comparing hydrogen and gasoline fires. Furthermore, improving this innovation and technology will drive the sustainable energy revolution towards achieving NZE goals.

Keywords: Transportation Emissions, Geoscience, Hydrogen Energy, Green Hydrogen

Introduction

Motor vehicles are the driving force behind global transportation, but they account for 10% of total emissions, as seen in the International Energy Agency (IEA) report (2023). The reliance on fossil fuels underscores the need to address greenhouse gas (GHG) emissions in the sector to achieve Net Zero Emissions (NZE). Pollutants from gaseous emissions, including carbon dioxide (CO_2), methane (CH_4), and nitrous oxide (N_2O), can linger in the Earth's atmosphere for decades, disrupting natural gas cycles and contributing to global warming (Massar et al., 2021). Furthermore, Indonesia's main contributor to this issue is petroleum-based fuels, which reached 448.53 million BOE (Barrels of Oil Equivalent) in 2023 (Ministry of Mineral Resources, 2023).

The long-term solution to replace the dependence on fossil fuels is to explore alternatives in automotive power. Despite the increased deployment of solar PV, wind energy, electric vehicles, and batteries, as well as the positive impact of updated Nationally Determined Contributions (NDCs), global CO_2 emissions from the energy sector peaked in 2022. Current projections indicate a potential global warming of 2.4 °C by 2100, far exceeding the 1.5 °C target outlined in the Paris Agreement (IEA, 2023). This highlights a significant gap between existing efforts and the ambitious goals of the NZE scenario, necessitating more aggressive actions and enhanced international cooperation to accelerate the transition to a sustainable, low-carbon future.

Green hydrogen, generated from renewable sources including wind, solar, or hydroelectric power, produces zero GHG emissions. It is an excellent option for reducing carbon footprints and addressing climate change. Moreover, it provides a significant opportunity for storing renewable energy, offering a solution for periods when solar or wind resources are unavailable. Surplus renewable energy during peak production can be converted into hydrogen via electrolysis and stored for later use.

This type of hydrogen shows great promise as a future fuel for road transportation. Compared to conventional production, it is projected to achieve zero carbon emissions throughout its entire lifecycle, from production to use. It is theoretically the greenest combustion product, producing only non-polluting water. Hydrogen has strength in its parameters, as shown in Table 1, unlike gasoline and diesel. The high calorific value and octane number of hydrogen enable it to function efficiently at high compression ratios, releasing more energy for the same mass (Sun et al., 2023). In the automotive sector, hydrogen-fueled internal combustion engines have regained attention due to their similarities in principles and minimal structural differences compared to gasoline and diesel engines (Sun et al., 2023). Therefore, as green hydrogen is integrated into vehicle power systems, reliance on fossil fuels will diminish, reducing global carbon emissions.

Table 1. Characteristics of Hydrogen

Characteristics	H2
Carbon content	0%
Density	0.089 g/L
Boiling point	-252.77 °C
Triple point	-254.4 °C
Autoignition temperature	858 K
Gas-liquid volume ratio (15°C, 100 kPa)	974 L/L
Critical pressure	1.29 MPa
Diffusion coefficient	0.61 cm^2/s
Minimum ignition energy	2 x 10^{-5} J
Calorific value	1.43 x 10^8 J/Kg
Volumetric energy density	10.7 MJ/m^3
Concentration of combustible	4% - 75%
Equivalent air-fuel ratio	34.5
Adiabatic flame temperature (air)	2254 °C
The maximum flame propagation speed	2.91 m/s
Octane number	130
Quenching distance	0.64 mm
Explosive level	Level 1
Flammability level	Level 4
Toxicity level	Level 0

Source: Adapted from Sun et al. (2023).

A study conducted in 2023 in Thailand confirmed hydrogen's potential in decarbonising the nation's energy system, presenting it as a viable solution for reducing GHG emissions in

fields where electrification and energy efficiency are less feasible (Pradhan et al., 2024). The findings indicate a need for nationwide renewable energy and green hydrogen production from 2031 to 2050. However, the study did not address innovations required to meet the NZE solution.

The study highlights Enhanced Geothermal Systems (EGS) as an innovative renewable heat source for the electrolysis process in green hydrogen production by evaluating green hydrogen's role in transportation and leveraging geoscientific methods. EGS provides a consistent energy supply with low environmental impact, enhancing energy sustainability and optimising infrastructure site selection through geoscience.

Given this context, this research aims to bridge the geoscientific gap by utilising EGS to produce green hydrogen, providing a viable solution for meeting NZE targets in the road transportation sector. This paper will use bibliometric analysis to focus on the manufacture of green hydrogen through EGS and the application of hydrogen fuel in vehicle engines. It is important to note that the researchers did not create the materials discussed in this paper. However, a comprehensive bibliography has been provided to properly credit the extensive sources and references that inform this work.

Theoretical Framework

Net Zero Emissions

NZE refer to the condition in which the metric-weighted anthropogenic GHG emissions are balanced by metric-weighted anthropogenic GHG removals over a specified period (IPCC, 2021). Achieving this balance demands substantially reduced GHG emissions, primarily by shifting from fossil fuels to renewable energy sources. Key strategies include increasing the use of renewable energy, decreasing energy consumption, and deploying carbon capture and storage innovation. The path to net zero involves the following approach: reducing carbon emissions as much as possible and using carbon removal technologies to neutralise any remaining emissions.

Automotive Energy Source

In this context, energy sources refer to various forms of energy used to power road vehicles. These sources are generally categorised into renewable and non-renewable. Fossil fuels (coal, natural gas, and oil) have been widely used for energy production and are expected to remain the leading energy source unless serious action is implemented to transition. With global primary energy demand increasing by 1.3% annually until 2040, these fossil fuel reserves will become increasingly scarce, especially as global transport relies almost entirely (>99%) on combustion engines burning liquid petroleum fuels (Megia et al., 2021; Kalghatgi et al., 2018).

Fossil fuels are considered the best energy sources for on-road vehicles due to their high gravimetric and volumetric energy density, which makes HC fuels particularly efficient (Yu et al., 2020). Another advantage of engines running on HC fuels is that the oxidiser and the

working fluids are freely available without adding extra cost or weight to the vehicle (Yu et al., 2020). However, as one of the world's largest consumers of petroleum-based energy, the transportation sector continues to generate significant GHG emissions.

Hydrogen

Hydrogen (H_2) is known as the lightest and simplest element, consisting of just one electron and one proton. The existence of this planet is abundant, primarily in water and organic compounds. It is a colourless, odourless, and flammable gas (Dawood et al., 2020). Furthermore, hydrogen can be produced from a variety of resources, including both fossil fuels and renewable sources (Dawood et al., 2020). According to Velazquez Abad and Dodds (2020), hydrogen that meets specific sustainability criteria is referred to as 'green' hydrogen. This criteria focuses primarily on limiting GHG emissions during its production. To be considered "green," hydrogen must be produced using processes that typically involve renewable energy and meet strict emission thresholds, ensuring minimal environmental impact.

Traditional, low-CO_2, CO_2-free, and carbon-free production methods are commonly categorised by the colour terms 'grey,' 'blue,' 'turquoise,' and 'green,' as shown in Fig. 1 (Hermesmann et al., 2022). Moreover, the colour categories are illustrated using various production technologies. Steam methane reforming (SMR) produces 'grey' hydrogen. Hydrogen obtained through SMR with carbon capture and storage is classified as 'blue.' Methane pyrolysis yields 'turquoise' hydrogen, while polymer electrolyte membrane water electrolysis produces 'green' hydrogen (Hermesmann et al., 2022).

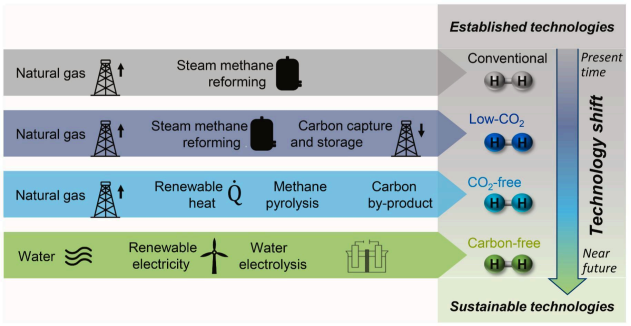

Figure 1. Common classification of hydrogen production pathways into conventional, low CO_2, CO_2-free, and carbon-free methods, along with their frequently associated colours. Adapted from Hermesmann, M., & Müller, T. E. (2022).

Hydrogen as an Energy Source

Hydrogen is significantly more diffusive than natural gas and gasoline, about four times more than natural gas and twelve times more than gasoline, due to its low density, which is only 6.9% that of air (Singh et al., 2015). This high diffusivity means that the gas quickly disperses upward in the event of a hydrogen leak, reducing the risk of fire or explosion. Also, a leak would not harm the environment since hydrogen is non-toxic. However, hydrogen

could pose a fire or explosion hazard in enclosed spaces if it mixes with air. Any resulting fire would be extinguished quickly as the hydrogen dissipates. Although a hydrogen-air mixture can ignite with a spark, it is more likely to burn rather than explode in open air. Some literature suggests hydrogen-powered vehicles may be safer than gasoline-powered ones in confined spaces, as gasoline leaks create larger flammable gas clouds.

In energy shift, an engine that uses hydrogen as energy operates close to a conventional internal combustion engine (ICE) (Gurz et al., 2017). It ignites the fuel mixture, causing it to burn and expand in the combustion chamber, which drives the piston and turns the crankshaft through the crank linkage. This process converts chemical energy into mechanical energy for external use. Moreover, as a renewable energy source, hydrogen can be used alone as a fuel in ICEs or as an additional fuel by blending it with fossil fuels.

Enhanced Geothermal System (EGS)

Enhanced Geothermal System (EGS) is a geothermal technology that extracts heat within the Earth's crust by artificially enhancing the permeability of hot rock formations. This is achieved by creating a network of fractures in the rock, allowing water to circulate through the system, absorb heat, and then be brought to the surface for electricity generation. EGS can be developed in various geological settings, making it a versatile option for expanding geothermal energy production. Traditionally, significant hydrothermal resources have been essential for extensive geothermal power generation. The process begins with identifying a reservoir, extracting the contained fluid, and converting the geothermal energy into electricity (Van Der Meer et al., 2014). However, similar to oil reserves, these reservoirs are limited and lessen as fluids are extracted. Gallup (2009) describes EGS as extracting heat from 'tight' rock formations lacking natural fractures and poor permeability. This technology enhances or creates permeability of hot rock formations, enabling fluid circulation to extract heat from the rock (Sharmin et al., 2023). Sharmin et al. (2023) emphasise that EGS offers a viable option for enhancing its capability of conventional geothermal systems. As a sustainable energy source, EGS has the potential to contribute significantly to the global energy landscape.

Setting up an EGS facility involves fulfilling certain requirements. These include having accessible thermal energy within a few kilometres of the Earth's surface and creating a network of fractures for fluid circulation. The process starts with locating an appropriate site where rock temperatures are sufficiently high at depths of 4-5 kilometres. Unlike typical geothermal reservoirs, the emphasis is on locating dry, extremely hot rock, greatly expanding the number of prospective sites for EGS technology. Following site selection, wells are drilled into the hot rock, which is then treated to develop fractures robust enough for fluid injection and circulation. The fluid passes along these newly formed routes, collecting heat before being extracted via production wells. This hot fluid is transported to the surface, used to generate electricity at a power station, and then returned via injection wells to be reheated, resulting in a closed-loop system. The basic layout of an EGS-type geothermal plant, which facilitates this process, is depicted in Fig. 2. Furthermore, if the plant operates a closed-loop binary cycle for electricity generation, no fluid is released into the environment, leading to

zero greenhouse gas emissions and only water vapour from the cooling systems (Olasolo et al., 2016).

Heat Extraction

Heat extraction is an important aspect of EGS that involves the recovery of thermal energy from geothermal reservoirs to generate power. This process is done by circulating a working fluid, typically water or CO_2, through the reservoir to capture heat and transport it to the surface. In EGS, heat extraction is accomplished by continuously circulating the working fluid between the injection and production wells. This fluid is injected into the geothermal reservoir at a lower temperature and pressure, absorbing heat from the surrounding hot rocks. It then travels to the production well, extracting it for power generation or direct heating purposes (Zhao et al., 2023).

The effectiveness of heat extraction is affected by several factors, including the geothermal reservoir's temperature, capacity, and permeability. Selecting optimal sites for heat extraction requires a comprehensive exploration process that involves inventorying surface manifestations, conducting geological and hydrogeological surveys, performing geochemical analysis, and carrying out geophysical surveys (Sharmin et al., 2023). The design of the production well is essential for maximising the extraction of the heated fluid, ensuring a stable flow rate and temperature. Key considerations include the wellbore's diameter, depth, and any obstructions or fractures that could impede fluid flow. Moreover, the temperature gradient within the reservoir is crucial for determining the heat extraction rate (Zhao et al., 2023).

In EGS, the idea of storage refers to the geothermal reservoir's capacity to retain heat and preserve its thermal characteristics over time. The storage capacity is crucial for the long-term viability of EGS. It is affected by factors such as the reservoir's volume, porosity, permeability, and the thermal conductivity of the rock matrix (Zhao et al., 2023). Effective management is required to avoid thermal depletion, ensuring the reservoir's heat is either replenished or its natural recharge abilities are enhanced.

Methods

The researchers in this paper use the mixed-method approach with an explanatory sequential design, combining quantitative analysis and a comprehensive literature review. First of all, the researchers use bibliometric analysis to analyse publication trends and identify influential research related to the topic, followed by reviewing technical reports to evaluate the impact and content of previous studies. This will lead to a broad overview of the research environment to point out the literature gaps. The analysis also provides the key trends and influential papers from previous studies. Furthermore, the researchers can explore deeper technical reports, allowing them to identify research gaps.

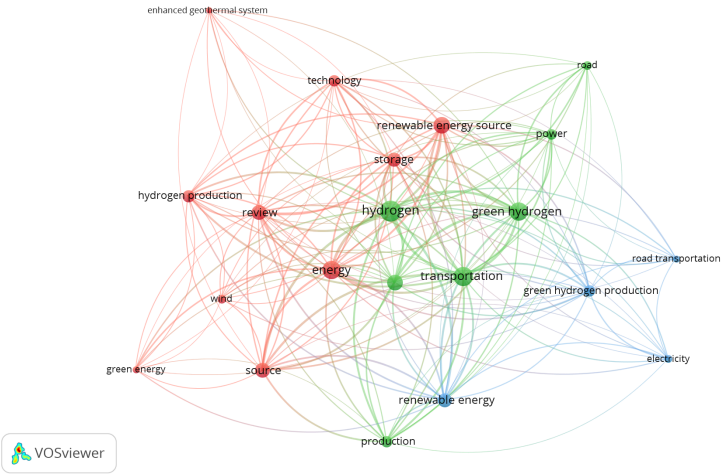

Figure 2. Network visualisation of keywords on hydrogen research (2014-2024).

Figure 2 illustrates the network visualisation map of author keywords in hydrogen research during the investigation period, which was analysed using VOSviewer's citation analysis. The largest cluster, highlighted in green, includes the terms "hydrogen," "green hydrogen," and "transportation." The analysis reveals that green hydrogen serves as a comprehensive term encompassing all advancements in road transportation energy. There is a significant emphasis on the production, storage, and technological aspects required to advance hydrogen as a key energy source. Peripheral topics like wind energy and electricity suggest that alternative or complementary energy sources are also considered within the broader research context. Additionally, the map identifies a nexus between EGS and green hydrogen, prompting the researchers to explore their potential synergy in revolutionising energy solutions for road transportation.

Table 2. Table of Research Variable Definition.

Variable Type(s)	Variable Name(s)
Independent Variable	Green hydrogen
Dependent Variable	Carbon emissions reduction Automotive energy efficiency
Control Variable	Production technology quality Infrastructure limitations
Confounding Variable	Green hydrogen production process

Source: Authors' Analysis, 2024

Based on the study's objectives and bibliometric analysis, Table 2 outlines the variables for qualitative research. These variables can be further explained, with green hydrogen serving as the key factor influencing the dependent variable. Green hydrogen is harnessed through EGS

and is explored as an alternative fuel for automotive applications. To propose green hydrogen as the pioneering solution in alternative energy, comparisons are drawn with grey hydrogen. The employment of hydrogen fuel in ICEs is also reviewed to assess the efficiency.

The researchers controlled the key variables to ensure that the effects on carbon emissions reduction and energy efficiency were due to green hydrogen itself. Production technology quality was standardised to ensure improvements were not simply due to better technology. Infrastructure limitations were also controlled to focus on green hydrogen's intrinsic properties, preventing external factors from influencing the results. While the green hydrogen production process could potentially affect outcomes, it was kept constant throughout the study.

Data and Results

Green Hydrogen as a Sustainable Alternative Fuel

Hydrogen is known as one of the most promising sustainable alternative fuel sources. Nevertheless, the overall sustainability is determined by the method of production. In industry, there are several processes for generating hydrogen gas. “Grey” hydrogen is known as the most common hydrogen assembly. It is produced from fossil fuels, such as coal or natural gas.

On the other hand, this process has significant environmental disadvantages, mostly because of its substantial carbon dioxide (CO_2) emissions. For every 1 kg of grey hydrogen produced, approximately 10 kg of CO_2 is released into the atmosphere (Suleman et al., 2015). However, another environmentally friendly option is acknowledged as green hydrogen. This type of hydrogen is produced through the electrolysis of water using renewable sources such as wind or solar power. Using this method, the production process is totally free of emissions. This makes green hydrogen a clean and highly sustainable energy source.

One of the most used processes for grey hydrogen is steam methane reforming (SMR) of natural gas. This process produces hydrogen together with CO_2 emissions, using non-renewable resources, i.e., fossil fuels. On the flip side, green hydrogen is produced through electrolysis. This method uses the sodium chlorine cycle powered by renewable electricity sources such as wind and solar for production. Due to this, green hydrogen minimises the environmental impact compared to grey hydrogen.

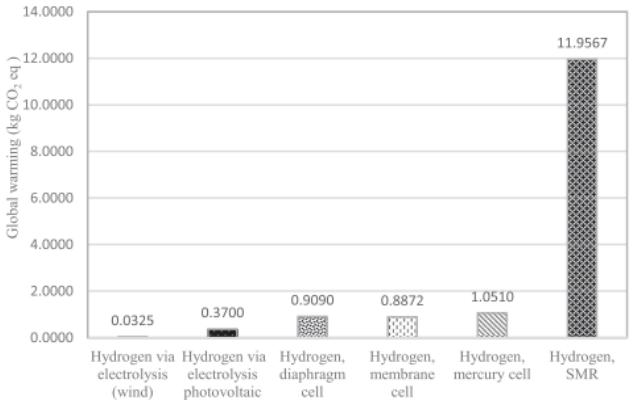

Figure 3. Global warming potential per kilogram of hydrogen for various hydrogen production methods. Adapted from Suleman et al. (2015).

SMR has a value of 11.9567 kg CO_2-eq compared to other hydrogen production methods. This is so extreme compared to wind-based electrolysis production methods with a value of just 0.0325 kg CO_2-eq. This data demonstrates that hydrogen production with renewable energy sources has greater environmental advantages than fossil fuels. Grey hydrogen using fossil fuel and green hydrogen using renewable energy are the main methods that we analyse in this research. We examine the most notable environmental effects, i.e., global warming potential. From the results shown, we can conclude that natural gas steam methane reforming (SMR) has the greatest environmental effects in both areas, highlighting the need for more sustainable options, such as green hydrogen.

Addressing green hydrogen is inseparable from their proven technique for storing green hydrogen. This technique implements the natural flexibility and impermeability of geological formations in salt caverns and depleted oil fields on a large scale for a long amount of time. According to information from the Advanced Clean Energy Storage Hub in Utah, this technique involves combining distribution for decarbonisation and grid stabilisation and utilising secure salt cavern storage. It produced green hydrogen by electrolysis powered by renewable energy sources such as wind. Also, this proven technique is crucial for encouraging the transition to a sustainable energy system with lower carbon emissions, even with issues like expensive starting costs and reduced efficiency.

As a result, green hydrogen is now recognised as a sustainable alternative fuel. The use of renewable energy sources in electrolysis assures that there will be a minor environmental impact from the manufacture of green hydrogen to its usage. Green hydrogen is a superior alternative energy source due to its entire life cycle.

EGS as A Key Innovation in Hydrogen

EGS represents a leading innovation in geothermal energy, offering unparalleled efficiency in electricity generation compared to other geothermal systems. EGS could also provide a sizable portion of the low-temperature thermal energy used because, despite being less common than other more widespread geothermal systems worldwide, they have a greater

capacity to produce electricity (Reber et al., 2014). Table 2 provides forecasts for expected electricity production capacity in the near future.

According to Chidire, Schifflechner, and Massier (2023), the process of hydrogen production through electrolysis, powered by heat extracted from an EGS, is a sustainable and environmentally friendly method that holds promise for the future of energy. In this system, geothermal energy is harnessed by circulating a heat transfer fluid through a closed-loop heat exchanger that extends deep into the Earth's crust, where it absorbs heat from the surrounding rocks without direct contact. This heat is then used to drive an Organic Rankine Cycle (ORC), which efficiently converts thermal energy into electricity, as depicted in Figure 4.

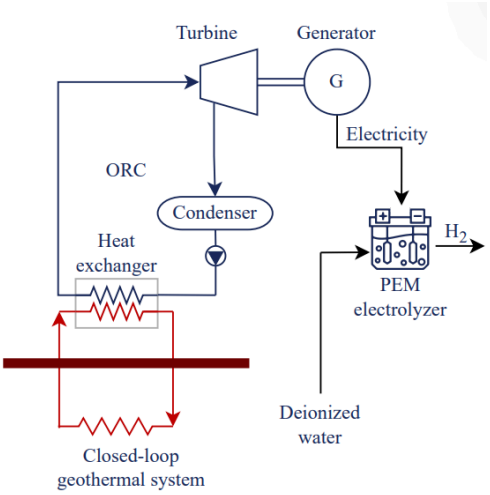

Figure 4. Closed-loop hydrogen production system powered by geothermal energy. Adapted from Chidire et al., (2023).

EGS technology is particularly significant in the pursuit of NZE due to its outstanding environmental benefits. According to the Intergovernmental Panel on Climate Change (IPCC, 2011), EGS power plants are likely to be designed with zero direct emissions, and life cycle assessment studies estimate that their total GHG emissions are less than 80 g CO_2eq per KWH, making them suitable for deep decarbonisation of the power sector (Goldstein et al., 2011). EGS systems produce minimal atmospheric emissions, with advanced closed-loop and binary systems achieving near-zero emissions compared to traditional fossil fuels. This positions EGS as a crucial technology for reducing greenhouse gases and achieving NZE targets.

Compared to other electricity generation options, EGS offers distinct advantages, unlike solar and wind, which are intermittent and require battery storage (U.S. Energy Information Administration, n.d.). EGS provides a stable and continuous energy supply. While natural gas remains a baseload power source, it is still dependent on fossil fuels. EGS-driven electrolysis, however, produces clean hydrogen with a low Global Warming Potential (GWP) of 3.67 kg CO_2eq per kilogram of hydrogen produced, significantly lower than other hydrogen production methods. This positions EGS-driven electrolysis as vital to global energy transitions and NZE goals (Chidire et al., 2023).

Hydrogen Employment in Internal Combustion Engines (ICEs)

Hydrogen energy is considered to be a renewable energy that can help internal combustion engines (ICEs) achieve lower emissions. The operation of a hydrogen engine is similar to that of a traditional ICE through the carburettor or injection system, similar to gasoline. However, minor modifications to the current gasoline combustion structure and system may be needed to adapt the engine for compatibility with hydrogen energy (Dincer & Acar, 2015). The three main types of alternative combustion strategies in ICEs are fuel carburetion, port fuel injection (PFI), and direct injection (DI) (Catapano et al., 2016). Figure 5 showcases the diagrams of the processes.

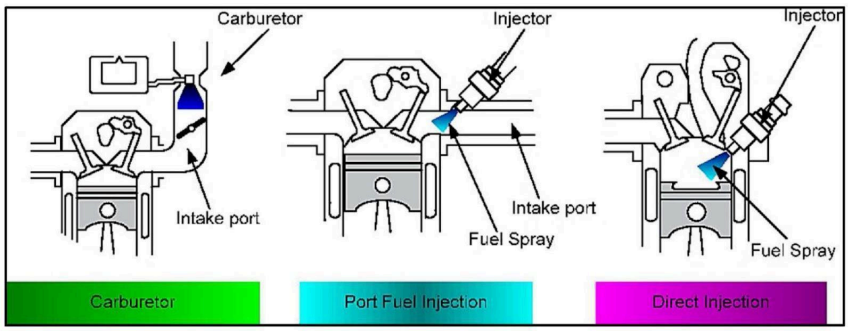

Figure 5. Engine hydrogen utilisation techniques. Adapted from Roy & Pramanik (2024).

Roy and Pramanik (2024) mention the main techniques of hydrogen in ICEs in their paper. The first type, fuel carburetion, is considered the most conventional and efficient method. Typically, hydrogen fuel flows into the intake manifold, where it blends with air before moving into the engine through the inlet valve. The throttle valve controls the number of hydrogen-air mixture supplied to the engine. Converting a standard gasoline engine to run on hydrogen will be relatively simple, as the engines are often equipped with a carburettor.

Following this, PFI for Spark Ignition Engines (SIE) fuel is a technology that is injected into the intake port, where it mixes with air. This air-hydrogen mixture then passes via the inlet valve during the engine's intake stroke. Due to hydrogen's low combustion energy and short flame quenching distance, PFI combustion is susceptible to pre-ignition, knocking, and backfiring (Roy & Pramanik, 2024). Lastly, the DI is a device that is similar to traditional compression ignition engines, where hydrogen fuel is injected above the cylinder head. Due to its excellent diffusion properties, hydrogen rapidly merges with the combustion air, and a spark plug can serve as the flame source.

Assessing Hydrogen's Role as a Fuel in ICEs

ICE technology powered by ethanol, methanol, and hydrogen is increasing, along with the rise of battery electric vehicles (BEVs) and fuel cell electric vehicles (FCEVs) (Pardo-Garcia et al., 2021). Each classification has its specific advantages and challenges that are classified for different applications. BEVs are ideal for urban transportation due to their short-range capabilities, whereas FCEVs perform better in longer ranges. However, hydrogen-fueled vehicles could offer more flexible solutions compared to BEVs and FCEVs. As diesel vehicles decrease, the H2-ICE system could offer a viable option, especially for medium and

heavy-duty vehicles. Unlike fuel cells, which require highly pure hydrogen, H2-ICEs can operate with less purity.

Regarding the efficiency of ICEs, an analysis by Gurz et al. highlighted the performance that uses hydrogen as the primary fuel (H2ICEs) (Gurz et al., 2017). The power efficiency of ICEs using premixed hydrogen, known as port-fuel injection H2ICE (PFI-H2ICE), is generally lower than that of engines fueled with gasoline or diesel. Their report has focused on improving the power efficiency of hydrogen engines, which has shown promise for the future of hydrogen-fueled ICEs. Researchers and companies like Ford and BMW have made notable advancements. For instance, Ford developed supercharged versions of the Zetec (4 cylinders, 2.0 L) and Duratec (4 cylinders, 2.3 L) engines for conventional and hybrid vehicles. Additionally, two Nissan engines designed for this purpose have increased power density and reduced NOx emissions. In hydrogen engines, NOx formation is influenced by the temperature and pressure in the combustion chamber, which can be managed using strategies like multi-mode operation and intercoolers, as seen in Ford's test engines. These developments are expected to improve the future of hydrogen ICEs further.

Another approach to narrow pollutant emissions involves advancing ICE technologies through the use of alternative energy and fuel blends, a topic reviewed in a study by Wróbel et al. (Wróbel et al., 2022). Blends such as ethanol, methanol, or water for gasoline engines and ethanol or glycerol-based ethers for diesel engines have shown considerable results. Additionally, this development allows hydrogen to be used as a fuel additive in conventional ICEs. Hydrogen's unique properties, such as low ignition energy, a wide flammability limit, and a fast combustion rate, make it an effective additive. It quickly fills the combustion chamber, forming a hydrogen-air mixture that ignites with minimal energy and burns more efficiently than hydrocarbon fuels. This results in improved combustion parameters, fewer unburnt residues, and higher combustion temperatures, leading to better energy conversion efficiency. For compression ignition engines, high-temperature hydrogen auto-ignition requires spark plugs or pre-ignition with a small amount of diesel fuel. Studies indicate that blending hydrogen with gasoline positively impacts exhaust emissions and efficiency.

Table 3. Comparative overview of H2-ICE, FCEV, and BEV

Aspect	H2-ICE	FCEV	BEV
Fuel & Source	Hydrogen (medium purity)	Hydrogen (high purity)	Electricity
Range	Medium-long	Long	Short-medium
Efficiency	Moderate	High	High
Emissions	NOx	No combustion emissions	No combustion emissions

Source: Author's Analysis, 2024

Conclusion

Based on the findings and analysis presented earlier, as well as the methodological approach taken to contextualise the research background, the researchers have reached the following conclusions: green hydrogen, produced through renewable-powered electrolysis, is a leading sustainable alternative fuel with minimal environmental impact, offering a cleaner option for road transportation via H2-ICEs and FCEVs due to its low ignition energy and high combustion efficiency. EGS represent a major advancement in geothermal energy, providing higher efficiency in electricity generation and, when coupled with electrolysis, achieving a Global Warming Potential (GWP) of 3.67 kg CO_2-eq per kilogram of hydrogen, significantly lower than other hydrogen production methods, thereby initiating a key technology in the global energy transition towards NZE. This paper outlines the significant potential benefits and areas for future development. However, it also recognises the persistent limitations and gaps in the existing body of research that need to be addressed.

References

A. Chidire, C. Schifflechner and T. Massier, "Life cycle assessment of green hydrogen production via geothermal energy-driven electrolysis," 2023 IEEE PES Innovative Smart Grid Technologies - Asia (ISGT Asia), Auckland, New Zealand, 2023, pp. 1-5, doi: 10.1109/ISGTAsia54891.2023.10372686.

Cao, W., Huang, W., Wei, G., Jin, Y., & Jiang, F. (2019). A numerical study of non-Darcy flow in EGS heat reservoirs during heat extraction. Frontiers in Energy, 13, 439-449.

Catapano, F., Di Iorio, S., Sementa, P., & Vaglieco, B. M. (2016). Analysis of energy efficiency of methane and hydrogen-methane blends in a PFI/DI SI research engine. Energy, 117, 378-387.

Conteh, C., Greitens, T. J., Jesuit, D. K., & Roberge, I. (Eds.). (2014). *Governance and public management: Strategic foundations for volatile times*. Routledge.

Dawood, F., Anda, M., & Shafiullah, G. M. (2020). Hydrogen production for energy: An overview. International Journal of Hydrogen Energy, 45(7), 3847-3869.

Dincer, I., & Acar, C. (2015). Review and evaluation of hydrogen production methods for better sustainability. International journal of hydrogen energy, 40(34), 11094-11111.

EIA, U.S., International energy outlook 2011. U.S. Energy Information Administration, 2011.

ESDM Ministry of Mineral Resources (2023). Handbook of Energy & Economic Statistics of Indonesia 2023.

Farah Nadiah, N. (2022). *Waste biomass assisted synthesis of silicon nanostructures for photoelectrochemical water splitting/Farah Nadiah Nordin* (Doctoral dissertation, Universiti Malaya).

Feldpausch-Parker, A. M., Endres, D., Peterson, T. R., & Gomez, S. L. (Eds.). (2022). *Routledge Handbook of energy democracy*. Routledge, Taylor & Francis Group.

Gallup, D. L. (2009). Production engineering in geothermal technology: A review. Geothermics, 38(3), 326–334. https://doi.org/10.1016/j.geothermics.2009.03.001

Gurz, M., Baltacioglu, E., Hames, Y., & Kaya, K. (2017). The meeting of hydrogen and automotive: A review. International journal of hydrogen energy, 42(36), 23334-23346.

Goldstein, B., G. Hiriart, R. Bertani, C. Bromley, L. Gutiérrez-Negrín, E. Huenges, H. Muraoka, A. Ragnarsson, J. Tester, V. Zui, 2011: Geothermal Energy. In IPCC Special Report on Renewable Energy Sources and Climate Change Mitigation [O. Edenhofer, R. Pichs-Madruga, Y. Sokona, K. Seyboth, P. Matschoss, S. Kadner, T. Zwickel, P. Eickemeier, G. Hansen, S. Schlömer, C. von Stechow (eds)], Cambridge University Press, Cambridge, United Kingdom and New York, NY, USA.

Hassan, Q., Sameen, A. Z., Salman, H. M., Jaszczur, M., Al-Hitmi, M., & Alghoul, M. (2023). Energy futures and green hydrogen production: Is Saudi Arabia trend?. *Results in Engineering*, *18*, 101165.

Heidinger, P. (2010). Integral modeling and financial impact of the geothermal situation and power plant at Soultz-sous-Forêts. Comptes Rendus Géoscience, 342(7–8), 626–635. https://doi.org/10.1016/j.crte.2009.10.010

Hermesmann, M., & Müller, T. E. (2022). Green, turquoise, blue, or grey? Environmentally friendly hydrogen production in transforming energy systems. Progress in Energy and Combustion Science, 90, 100996.

IEA (2023), Net Zero Roadmap: A Global Pathway to Keep the 1.5 °C Goal in Reach, IEA, Paris https://www.iea.org/reports/net-zero-roadmap-a-global-pathway-to-keep-the-15-0c-goal-in-reach, Licence: CC BY 4.0

IEA, IRENA & UN Climate Change High-Level Champions (2023), Breakthrough Agenda Report 2023, IEA, Paris https://www.iea.org/reports/breakthrough-agenda-report-2023, License: CC BY 4.0

Inderwildi, O., & King, S. D. (2012). Energy, Transport, & the Environment. *Springer, Berlin*, *10*, 978-1.

Kalghatgi, G., Levinsky, H., & Colket, M. (2018). Future transportation fuels. Progress in Energy and Combustion Science, 69, 103-105.

Karaca, A. E., & Dincer, I. (2023). Development of a new photoelectrochemical system for clean hydrogen production and a comparative environmental impact assessment with other production methods. *Chemosphere*, *337*, 139367.

Karagöz, Y., Sandalcı, T., Yüksek, L., Dalkılıç, A. S., & Wongwises, S. (2016). Effect of hydrogen–diesel dual-fuel usage on performance, emissions and diesel combustion in diesel engines. Advances in Mechanical Engineering, 8(8), 1687814016664458.

Massar, M., Reza, I., Rahman, S. M., Abdullah, S. M. H., Jamal, A., & Al-Ismail, F. S. (2021). Impacts of autonomous vehicles on greenhouse gas emissions—positive or negative?. International Journal of Environmental Research and Public Health, 18(11), 5567.

Megía, P. J., Vizcaíno, A. J., Calles, J. A., & Carrero, A. (2021). Hydrogen production technologies: from fossil fuels toward renewable sources. A mini review. Energy & Fuels, 35(20), 16403-16415

Meyers, R. A. (2012). Encyclopedia of sustainability science and technology (Vol. 6). New York: Springer.

Okolie, J. A., Patra, B. R., Mukherjee, A., Nanda, S., Dalai, A. K., & Kozinski, J. A. (2021). Futuristic applications of hydrogen in energy, biorefining, aerospace, pharmaceuticals and metallurgy. International journal of hydrogen energy, 46(13), 8885-8905.

Olasolo, P., Juárez, M., Morales, M., D´Amico, S., & Liarte, I. (2016). Enhanced geothermal systems (EGS): A review. Renewable and Sustainable Energy Reviews, 56, 133–144. https://doi.org/10.1016/j.rser.2015.11.031

Pardo-García, C. E., Pabon, J. A., & Fonseca Vigoya, M. (2021). Effects on CO and CO2 emissions by direct hydrogen substitution in a compression ignition engine. International Review of Mechanical Engineering (IREME), 15(9), 504. https://doi.org/10.15866/ireme.v15i9.21557

Pradhan, B. B., Limmeechokchai, B., Chaichaloempreecha, A., & Rajbhandari, S. (2024). Role of green hydrogen in the decarbonization of the energy system in Thailand. *Energy Strategy Reviews*, *51*, 101311.

Reber, T. J., Beckers, K. F., & Tester, J. W. (2014). The transformative potential of geothermal heating in the U.S. energy market: A regional study of New York and Pennsylvania. Energy Policy, 70, 30–44. https://doi.org/10.1016/j.enpol.2014.03.004

Roy, A., & Pramanik, S. (2024). A review of the hydrogen fuel path to emission reduction in the surface transport industry. International Journal of Hydrogen Energy, 49, 792-821.

Shabaneh, R., RoyChoudhury, J., Braun, J. F., & Saxena, S. (2024). The Clean Hydrogen Economy and Saudi Arabia: Domestic Developments and International Opportunities (p. 803). Taylor & Francis.

Sharmin, T., Khan, N. R., Akram, M. S., & Ehsan, M. M. (2023). A state-of-the-art review on geothermal energy extraction, utilization, and improvement strategies: conventional, hybridized, and enhanced geothermal systems. International Journal of Thermofluids, 18, 100323.

Singh, S., Jain, S., Venkateswaran, P. S., Tiwari, A. K., Nouni, M. R., Pandey, J. K., & Goel, S. (2015). Hydrogen: A sustainable fuel for future of the transport sector. *Renewable and sustainable energy reviews*, *51*, 623-633.

Sinigaglia, T., Lewiski, F., Martins, M. E. S., & Siluk, J. C. M. (2017). Production, storage, fuel stations of hydrogen and its utilization in automotive applications-a review. International journal of hydrogen energy, 42(39), 24597-24611.

Solar and battery storage to make up 81% of new U.S. electric-generating capacity in 2024 - U.S. Energy Information Administration (EIA). (n.d.). https://www.eia.gov/todayinenergy/detail.php?id=61424

Sukarno, I., Matsumoto, H., & Susanti, L. (2016). Transportation energy consumption and emissions-a view from city of Indonesia. Future Cities and Environment, 2, 1-11.

Suleman, F., Dincer, I., & Agelin-Chaab, M. (2015). Environmental impact assessment and comparison of some hydrogen production options. International journal of hydrogen energy, 40(21), 6976-6987.

Sun, Z., Hong, J., Zhang, T., Sun, B., Yang, B., Lu, L., ... & Wu, K. (2023). Hydrogen engine operation strategies: recent progress, industrialization challenges, and perspectives. International Journal of Hydrogen Energy, 48(1), 366-392.

Van Der Meer, F., Hecker, C., Van Ruitenbeek, F., Van Der Werff, H., De Wijkerslooth, C., & Wechsler, C. (2014). Geologic remote sensing for geothermal exploration: A review. International Journal of Applied Earth Observation and Geoinformation, 33, 255–269. https://doi.org/10.1016/j.jag.2014.05.007

Wróbel, K., Wróbel, J., Tokarz, W., Lach, J., Podsadni, K., & Czerwiński, A. (2022). Hydrogen internal combustion engine vehicles: a review. Energies, 15(23), 8937.

Yu, X., Sandhu, N. S., Yang, Z., & Zheng, M. (2020). Suitability of energy sources for automotive application–A review. Applied Energy, 271, 115169.

Yue, M., Lambert, H., Pahon, E., Roche, R., Jemei, S., & Hissel, D. (2021). Hydrogen energy systems: A critical review of technologies, applications, trends and challenges. Renewable and Sustainable Energy Reviews, 146, 111180.

Zhao, W., Yuan, Y., Jing, T., Zhong, C., Wei, S., Yin, Y., Zhao, D., Yuan, H., Zheng, J., & Wang, S. (2023). Heat Production Performance from an Enhanced Geothermal System (EGS) Using CO2 as the Working Fluid. Energies, 16(20), 7202. https://doi.org/10.3390/en16207202

About the Organisers

1. Profile: Resilience Development Initiative (RDI)

Resilience Development Initiative (RDI) is a non-profit organization dedicated to promoting sustainable development and resilience-building efforts in communities facing challenges such as disasters, climate change, and social vulnerabilities. RDI collaborates with various stakeholders, including government agencies, NGOs, academic institutions, and community organizations, to design and implement innovative solutions for building resilience and mitigating risks.

At the core of RDI's approach is the integration of research, capacity-building, and community engagement to address complex issues related to disaster management, climate adaptation, and sustainable development. The organization emphasizes the importance of local knowledge and community involvement in developing effective strategies that are tailored to specific regional needs.

RDI's initiatives cover a wide range of areas, including disaster risk reduction, sustainable livelihoods, environmental conservation, and technology-driven solutions. Through partnerships with local and international entities, RDI strives to foster a collaborative network of stakeholders committed to enhancing resilience and ensuring the well-being of vulnerable communities.

The organization's efforts extend beyond immediate response and recovery, emphasizing long-term planning and development to create lasting and sustainable change. By harnessing the collective expertise and resources of its partners, RDI aims to empower communities to withstand and recover from various challenges, fostering a more resilient and adaptive future for the people and environments they serve.

For more information, please visit https://rdiglobal.org/

2. Profile: IUGC ITB 2024

International Undergraduate Geophysics Competition (IUGC) ITB is a competition event organized by Himpunan Mahasiswa Teknik Geofisika "TERRA" ITB. The event aims to introduce the importance of Geophysical Engineering in development and international competition, as well as raising awareness of the role of students in maintaining the sustainability of the earth.

The vision for this event is IUGC ITB 2024 to be a collaborative platform to foster innovation and knowledge to positively contribute to world issues. The IUGC ITB 2024 Event was designed to provide an in-depth understanding of the earth sustainable, introducing Net Zero Emission (NZE) concept, where the greenhouse gas emissions released into the atmosphere are proportional to the emissions that can be removed or compensated. Through a series of events consisting of talkshow & webinar, competitions, exhibition, community services, and awarding night that provide participants to gain insight into the science of geophysical engineering.


rdi
Resilience
Development
Initiative